NTNU

Norwegian University of
Science and Technology

# Modeling, simulation and implementation of Multi-phase Induction Motor Drives.

**Sachin Thopate**

Master of Energy Use and Energy Planning
Submission date: June 2011
Supervisor: Tom F. Nestli, ELKRAFT
Co-supervisor: Roy Nilsen, ELKRAFT

Norwegian University of Science and Technology
Department of Electric Power Engineering

NTNU – Trondheim
Norwegian University of
Science and Technology

# MODELING, SIMULATION AND IMPLEMENTATION OF MULTI-PHASE INDUCTION MOTOR DRIVES.

SACHIN SUBHASH THOPATE.

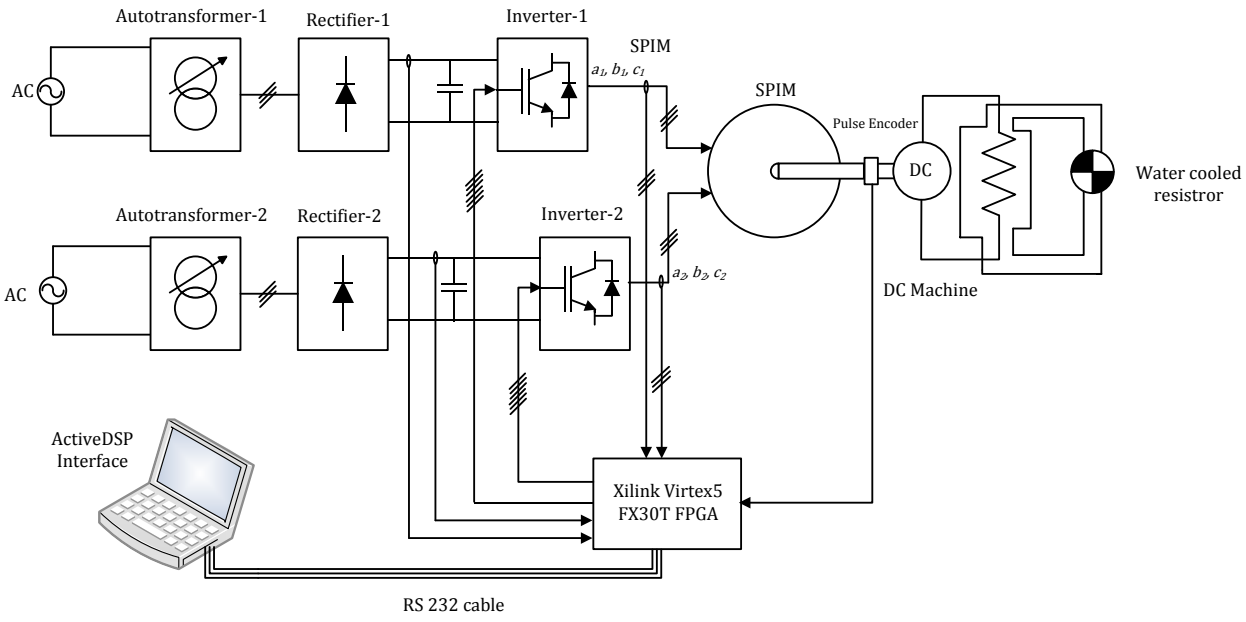


Master Thesis submitted to

***Norwegian University of Science and Technology.***
***Department of Electric Power Engineering.***

in partial fulfillment of the requirement for the
Degree of Master of Science in Electric Power Engineering.

**Supervisors**
Adj.Prof. Tom Nestli. ( Nescon AS)
Dr. Engg. Roy Nilsen.( Wärtsilä AS)

**Funding.**
Wärtsilä Norway AS.
**27th June 2011**.

**Problem Description.**

To increase the achievable power rating and to reduce cost of the drive system, both six and nine phase machines are of interest to be applied in ship propulsion. Today's typical maximum power rating today is 5 MW using three phase machines and low voltage drives.

This work is to be based on the candidates work during the specialization project. The candidate has studied the control strategy for a six phase induction motor and assembled a laboratory drive with such a machine.

In this master thesis work, the candidate shall:

- Program the FPGA control card for the Double Synchronous Frame Current Controller (DSFC) control strategy and compare the simulation results for different operating conditions with the actual results observed in the lab for the six phase induction machine.
- Implement and evaluate the new control method Decoupled Multi-phase Current Control method (DMCC)
- Investigate the effect of limiter functions in the different inverters. The current and dc-link voltage limiter functions are of particular interest.

If there is enough time, the candidate should model and discuss the control strategies for nine phase induction machine and simulate such a drive in SimPower.

**Supervisor**: Prof. Tom F. Nestli.

**Co-supervisor**: Roy Nilsen Wartsila Norway As.

## Preface.

My work in the multiphase motor drive started last year with a summer-job at Wärtsilä under guidance and supervision of Roy Nilsen, since then my learning curve in the multi phase motor drives is rising.

This thesis work of Modeling, Simulation and Implementation of Multi-phase Induction Motor Drives has been funded by the Wärtsilä. As I am actively associated with this project since last year I got a unique privilege to work alongside few experts in the electric drives and control field.

The task was not easy, however the excellent working atmosphere and cooperation from the university personnel made the task easy for me. The development of the six phase induction motor drive for the commercial exploitation is still ongoing.

The thesis work was supervised by Tom Nestli, I want to thank Tom for all the support.

The thesis work was co supervised by Roy Nilsen of Wärtsilä. I would like to extend my deepest gratitude towards Roy for all kind help and intellectual nurturance. The time I spent with him will definitely be more than useful for me in the future for the progression of my professional carrier.

Kjell Ljøkelsøy is another person who I would like to mention and thank here, without his technical support the task could have not been completed.

The support extended to the thesis work by the service lab team was excellent. I wish to thank Thor Lohse, Bård Ålmas and Vladimir Klubica for all the support.

Thanks to all my friends here in Norway for all their personal support and care.

And at last I would like to thank my loving mom and dad in my homeland for all back up they extended throughout the last two years.

**27 June 2011.**

**Sachin Subhash Thopate .**

## Abstract.

Electric ship propulsion offers numerous advantages such as improved and precise control of the shaft speed, increased manoeuvrability, increased fuel efficiency, reduced environmental impact, and quiet operation. Inverter controlled multiphase motor drives are having number of advantages over the three phase drives in the medium voltage medium power range.

The purpose of this project work is to continue the work in the last semester towards the practical realization of the Six Phase Induction Motor drive. The hardware and Inverters are ready. The

The main task of the thesis is to implement and evaluate the two control strategies, Double synchronous Frame current Control and Decoupled Current Control. The FPGA control card is programmed accordingly to implement these two control schemes.

It is found during actual operation of the drive that in the normal steady state working condition both the control strategies perform satisfactorily, however in case of the fault in the system i.e. trip of the one inverter or the loss of one DC link, the DFSCC control scheme keeps machine running as three phase whereas the DCC control scheme fails. This is found only when the machine is not heavily loaded.

The DCC control scheme is extremely good otherwise and gives comparable performance as DSFCC since it try to balance the currents in the both the inverters.

In case of the low DC link voltage operation both the control schemes responds more or less similarly. It is also found that DSFCC can start the drive with only one inverter in case of light load whereas DCC scheme is unable to start the drive.

## Figures

Figure 2-1 : Four Quadrant Drives for the MV and High Power Applications. 4
Figure 2-2 : Space Vector representation. 5
Figure 2-3 : Clark and Park transformations for three phases. 6
Figure 2-4 : Equivalent circuits of three phase Induction motor. 8
Figure 2-5 : Indirect vector control of three phase Induction motor. 9
Figure 3-1: Six Phase Induction Machine. 11
Figure 4-1. Different modulation techniques for SPIM. [10] 19
Figure 5-1: Block diagram of Double Synchronous frame Current Control. 24
Figure 5-2: Block diagram of the Decoupled Control Strategy 27
Figure 6-1: System Synoptic of the test rig. 28
Figure 6-2: The Program structure. 30
Figure 6-3 : The State Machine 32
Figure 6-4: FPGA Control card [17]. 33
Figure 6-5: Control Board. 36
Figure 6-6: LEM Current Transducers and sensed currents 37
Figure 6-7. Three phase IGBT Inverter. 38
Figure 6-8. DC Rectifier 39
Figure 6-9: The test drive set up 40
Figure 7-1 : Simulation results for the step change in the torque reference. 42
Figure 7-2 : Ramp input in the $i_q$ Real time DSP trace 42
Figure 7-3 : Oscillogram traces of the Actual Motor Currents 43
Figure 7-4: Simulation results of the step reduction in the inverter 2 for DSFCC 44
Figure 7-5 : DSP trace of machine currents 45
Figure 7-6: Oscillogram traces of the Actual Motor Currents 45
Figure 7-7: Trip of inverter 2. 46
Figure 7-8: The trip of inverter 1. 47
Figure 7-9: Current in the inverter of healthy phase group. 47
Figure 7-10: Simulation results for operation with different DC link 48
Figure 7-11: Different DC link Voltage operation 49
Figure 7-12: Line currents in the inverter with reduced DC link. 49
Figure 7-13 : Line currents of the other inverter 50
Figure 7-14: Start with single phase group of the SPIM. 51
Figure 7-15 : Trip of the inverter 1. DSP log. 52
Figure 7-16 : Trip of healthy inverter as recorded on oscilloscope. 53
Figure 7-17: Different DC link operation DCC strategy 53

## Tables.

Table 1: Acronyms used in report. ..... VI
Table 2: Subscripts. ..... VII
Table 3: Superscript. ..... VII
Table 4 : Parameters. ..... VIII
Table 5. Controller data calculated for the simulation ..... 13

## Acronyms.

| Acronyms | Explanation |
|---|---|
| VSI | Voltage Source Inverter. |
| SPIM | Six Phase Induction Machine. |
| HMI | Human Machine Interface. |
| PDS | Power Drive System. |
| IEC | International Electrotechnical Commission. |
| PPU | Power Prosessing Unit. |
| PWM | Pulse Width Modulation. |
| DSP | Digital Signal Processor. |
| FPGA | Field Programmable Gate Array. |
| SVPWM | Space Vector Pulse Width Modulation. |
| DSFCC | Double synchronous frame current control. |
| DCC | Decoupled Current Control. |
| RISC | Reduced Instruction Set Computing. |
| RAM | Random Access Memory. |
| ASIC | Application Specific Integrated Circuits. |
| CAN | Controlled Area Network |
| UART | Universal Asynchronous Receiver Transmitter. |
| MAC | Media Access Controller |
| MSPS | Million Samples Per Second |
| LVDS | Low Voltage Differential Signalling |
| IP | Intellectual Property |

**Table 1: Acronyms used in report.**

## Parameters.

Parameters subscript and superscript used in the report. Lowercase letters are used to indicate instantaneous values, bold characters are used for matrix and underline specifies space vectors, hat is used to denote the maximum values while up ~ is used to denote the estimated values.

| Parameters | Explanation |
|---|---|
| s | Stator parameters |
| r | Rotor parameters |
| SR | Parameters for both stator and rotor |
| d-q | Parameters refer to d-q axes. |
| z | Parameters in z axis |
| 0 | Parameters in zero axis |
| $z_1$,$z_2$ | Axes of z subspace |
| $0_1$,$0_2$ | Axes of zero subspace |
| N | Rated values |
| n | Base values |
| ph | Phase values |
| rms | Root mean square values |
| σ | Leakage coefficient. |
| h,m | Main , Magnetising |
| *II* | Feed-forward terms |

**Table 2: Subscripts.**

| Parameters | Explanation |
|---|---|
| s | Parameters referred to stator. |
| r | Parameters referred to rotor. |
| SR | Parameters for both stator and rotor. |
| $\Psi_r$ | Parameters in rotor flux oriented model. |
| “ | Transient |

**Table 3: Superscript.**

| Parameters | Explanation |
|---|---|
| $U$ | Voltage |
| $I$ | Current |
| $R$ | Resistance |
| $x, X$ | Inductance |
| $\Psi$ | Flux Linkage |
| $\theta_r$ | Rotor angular position |
| $\boldsymbol{\mathcal{T}}$ | Transformation matrix in [8] |
| $\boldsymbol{T}$ | Time constant |
| $t$ | Time |
| $\Omega$ | Mechanical angular velocity |
| $\omega$ | Electrical angular velocity |
| $n$ | Rotor speed. |
| M | Electrical torque , electrical torque in pu |
| $M_L, m_L$ | Load torque, load torque in pu |
| $p$ | Pole pairs |
| $P$ | Electrical power |
| $\wp$ | Base power |
| $M_n$ | Base torque |
| $f_{\Psi_r}$ | Frequency of the rotor flux linkage |

**Table 4 : Parameters.**

# Contents

**1. INTRODUCTION ..... 1**

**2. THREE PHASE INDUCTION MOTOR DRIVES- A BRIEF REVIEW. ..... 4**

2.1. POWER SUPPLY FOR HIGH PERFORMANCE DRIVES ..... 4
2.2. VECTOR CONTROL OF THREE PHASE INDUCTION MOTOR. ..... 5
2.2.1 Space Vectors. ..... 5
2.2.2 Clark and Park Transforms. ..... 6
2.3. EQUIVALENT CIRCUIT OF THREE PHASE INDUCTION MOTOR. ..... 7
2.4. INDIRECT VECTOR CONTROL OF THE INDUCTION MACHINE AND FLUX ESTIMATORS. ..... 9

**3. MODELLING OF SIX PHASE INDUCTION MACHINES. ..... 11**

3.1. VECTOR SPACE DECOMPOSITION. ..... 11
3.2. ELECTROMAGNETIC SYSTEM. ..... 12
3.3. MECHANICAL SYSTEM. ..... 13
3.4. TRANSFORMATION OF CO-ORDINATES. ..... 13
3.5. PER UNIT SYSTEM ..... 14
3.6. TRANSFORMED MODEL OF SPIM ..... 16

**4. CONTROL SCHEMES FOR SIX PHASE INDUCTION MACHINE. ..... 18**

4.1. CONVENTIONAL SVM TECHNIQUE. ..... 18
4.2. VECTOR SPACE DECOMPOSITION TECHNIQUE. ..... 18
4.3. VECTOR CLASSIFICATION TECHNIQUE ..... 18

**5. CONTROL SCHEMES EVALUATED FOR SIX PHASE MOTOR DRIVE. ..... 21**

5.1. DOUBLE SYNCHRONOUS FRAME CURRENT CONTROL. ..... 21
5.2. DECOUPLED CURRENT CONTROL. ..... 25

**6. SYSTEM SYNOPTIC AND DRIVE IMPLEMENTATION. ..... 28**

6.1. SOFTWARE IMPLEMENTATION. ..... 29
6.1.1 Program Structure. ..... 29
6.1.2 The State Machine ..... 29
6.1.3 Motor States. ..... 31
6.2. HARDWARE IMPLEMENTATION. ..... 33
6.2.1 FPGA Control card. ..... 33
6.2.2 FPGA IP Modules . ..... 36
6.2.3 Control board. ..... 36
6.2.4 Currents and voltages measurements. ..... 37
6.2.5 Rotor Position Measurement. ..... 37
6.2.6 Inverter Modules. ..... 38
6.2.7 Converter. ..... 39
6.2.8 Six Phase Induction Motor. ..... 39
6.2.9 Assembly of the drive. ..... 40

**7. COMPARISON OF SIMULATIONS AND ACTUAL RESULTS ON THE DRIVE . ..... 41**

7.1. INTRODUCTION. ..... 41

7.1.1 Normal operation with the step change in the torque reference for the both inervters. ..... 41

7.1.2 Normal operation with the same DC link voltages and the reduction in the torque reference of one of the inverter. ..... 44

7.1.3 Trip of one of the inverter. ..... 46

7.1.4 Operation with different DC link voltage for the Inverters . ..... 48

7.1.5 Start with single phase group of the SPIM. ..... 50

7.2. THE DCC STRATEGY. ..... 52

7.2.1 Trip of one of the inverter. ..... 52

7.2.2 Low DC link voltage operation ..... 53

7.2.3 Start with the single phase group. ..... 53

**8. SUMMERY AND CONCLUSION. ..... 54**

**9. FURTHER WORK. ..... 1**

**REFERENCES. ..... 2**

**APPENDIX. ..... 5**

# 1. Introduction

The interests in the multiphase machine started to increase in late 1960 when the inverter fed three phase drives were in the development stage. Engineers found problem of the low frequency torque ripple in the three phase machines due to the six step operation of the inverters. Analysis showed that the lowest frequency torque ripple harmonic in the n phase machine is caused by the time harmonics in the supply of the order $2n\pm1$. The best solution to overcome this problem was to increase the number of the phases.

In 1974 Nelson and Krause carried out simulation of 7.5 hp six phase motor fed with two six step inverters and showed that the torque pulsations in the machine is reduced as a result of the asymmetrical placement of the winding phase group [3]. Further investigation of the machine winding configuration and the mutual leakage inductances with different phase belt angle and pitch for the six phase synchronous machine was done by Schiferl and Ong [4] in 1983 they also showed that if the axes of two phase groups are displaced by $30^0$ the torque pulsation and the voltage harmonic distortion is minimum.

In 1984 Abbas and Christen carried out practical work on the six phase motor fed with the six step transistor inverter and showed that the air gap flux time harmonics of the order $6n\pm1$ ($n = 1,3,5\ldots$) are eliminated which resulted in the elimination of the six harmonic dominant torque component [5].

Research work was also carried out for the five phase motor by in 1979 by Danzer, however the third harmonic currents were found excessive when the machine was supplied by inverter [6].

Six phase induction motors when fed with the six leg inverter using the space vector modulation technique that uses 12 sides of the space vector polygon, produce the $5^{th}$ and $7^{th}$ harmonics in the space; these harmonics cancel each other in the space if the windings are wound for the $30^0$ shift in two phase groups. However these harmonics causes considerable loss in the stator at low speed. This issue was addressed in 1993 by Gopakumar and Ranganathan. It was proposed [13] to operate the six leg inverter as two three phase inverters operating on three phase space vector modulation technique in the lower speed range; and it was suggested that the operation of inverters afterwards will smoothly switch to the six phase operation as speed increases.

The six phase machine were always viewed as the six dimensional spaces of currents and vectors, which is quite obvious, and engineers were addressing the control of the six phase machine by trying to locate the space vector in the six dimensional space and then rotating it. This was making the control as well as the modelling of the six phase machine difficult. In 1994 Lipo and Zaho [8] showed that six dimensional spaces could also be think as the three mutually perpendicular subspaces each containing two perpendicular vectors. Based on this idea the inverter voltage vectors can be projected along these subspaces and the appropriate

voltage vector in the respective subspaces can be selected for the switching. This technique reduces the current harmonics in a particular (known as z) subspace which are responsible for losses in machine, as it do not take part in the electromechanical energy conversion.

Research on the multiphase machine is still ongoing, the research work carried out in multiphase motor drives over the span of last four decade has proven that the technical and economic advantages of the multiphase motor are superior than that of the three phase motor drives. Some of the advantages of the six phase drives are mentioned below.

- It can be shown [1] that for the same torque and same speed the stator copper losses for the six phase machines are 6.7 % less than the three phase machines.
- The space harmonics generated by the fundamental component of stator currents in six phase machines are of higher order and hence more attenuated as compared to the three phase machines which lead to reduced torque pulsations [1].
- Six phase machines have greater fault tolerance than their three phase counterparts [2].
- Current rating for the inverter switches are reduced for controlling the six phase machine of the same power as three phase which lead to reduction of the cost.

In the following thesis an attempt has been made to realize vector controlled six phase induction motor drive for the application to marine propulsion. Various control strategies exists for the six phase machine control, the technology status for the same is reviewed in the [2].

Two control strategies are discussed and implemented in the thesis work, one is Double Synchronous Frame Current Control and other is Decoupled Multiphase Current Control.

The synchronous current control strategy was proposed by Bakhshai and Jin [11] this method is described under the name vector classification technique as the space vector modulation technique is used for the control of the inverters. Two schemes are proposed in [11]. In first the voltage reference to two inverters are displaced $30^0$ with each other and having identical modulators. In second method the switching states of the two modulators are displaced $30^0$ with each other and whereas the reference voltage is kept common. In the thesis the former method is used for the control using the sinusoidal pulse width modulation with the third harmonic injection and with the split DC link.

The second control strategy with the decoupled control is proposed by Bojoi and Profumo in [14], it is proposed to control the d-q and $z_1$-$z_2$ subspace currents with the PI controllers.This control strategy however is implemented in the stationary reference frame. The same control strategy is also proposed in the rotor oriented reference frame in [12] for the PMSM. The aim of the control philosophy is to control the currents induced in the $z_1$-$z_2$ subspace.

Field orientation and high performance control of the drive requires high speed microcomputers to process the digital signals. It is also required to have adequate resolution of the signals with respect to the time and amplitude. Various DSPs are available nowadays

in the market to fulfil both the tasks, i.e. sampling and processing of signals on the single control card. Power consumption, cost, speed and the suitability of the hardware for the effective implementation of the process algorithm are some of the very important criteria of the effective drive design. FPGAs are proving good option in that respect because of their parallel processing and interchange ability in addition with the improved control. The suitable choice of the FPGA also allows developer to use the floating point processor instead of the integers, thus allowing flexibility and ease of development of the process algorithm in the higher level language such as C and C++.

For the realization of the six phase induction motor drive the Xilinx Virtex5 FPGA is used which provides adequate flexibility in terms of the implementation of the floating point processing, and compatibility for signal processing with high speed sampling.

The control and process algorithm needs to have communication channel to the HMI. There exist various standards for generic interfaces and device profiles for communication. Few of them are listed in the IEC standard 61800-7 for Adjustable speed electrical power drive systems. However in the thesis work for the realization of the six phase motor drive DRIVECOM standard is used.

For the development of the process algorithm software development platform SDK is used, which is based on the Eclipse. This platform is provided by the Xilinx.

For the realization of the drive asymmetrical six phase induction motor is used which is fed with two three phase IGBT based inverters. The inverters are fed with the two separate DC links. Two DC link ensures the redundancy in the system.

The thesis is divided in the four main parts. The first part contains relevant theory of the three induction machine vector control along with the space vectors and machine equivalent circuit description.

The second part is dedicated to the six phase machine modeling and control. In the third part the development of the drive system is documented along with software and hardware description; while in the fourth part the simulation and the practical results are compared and discussed.

# 2. Three Phase Induction Motor Drives- A Brief Review.

Three phase induction motors are the workhorse of the industry. The invention of the vector control in early seventies was the first step in the high performance control of the induction motors. Increase in ratings of power electronic components made it possible to push the ratings of the induction motor drive as high as 4 MW [B.1]. Subsequent section contains relevant discussion about vector controlled three phase induction motor drive.

## 2.1. Power supply for high performance drives.

Various inverter topologies exist for the drives ranging from few kilowatts to several hundred Megawatts. However CSI and VSI are main inverter configurations that are more commonly used for the high performance induction motor drives in the medium voltage and medium power range.

VSI supply controlled voltages waveform for the motor while CSI produces controlled currents. The PWM controlled CSI produce motor friendly waveforms and reliable short circuit protection and thus it is believed to be widely used for the high power drives. VSI are popular in the medium voltage medium power range generally employing IGBT which can switch above 16 kHz i.e. beyond audible noise. VSI also provides large bandwidth for the control; with sufficient DC link voltage, fast current control loops can be designed to produce waveform nearly ideal current source for the machine. The configuration and typical current waveforms are shown in the Figure 2-1. [B.1]

When the DC side is fed with the controlled rectifiers, it is possible to feed the power back to the lines during the breaking operation of the motor and recover the power.

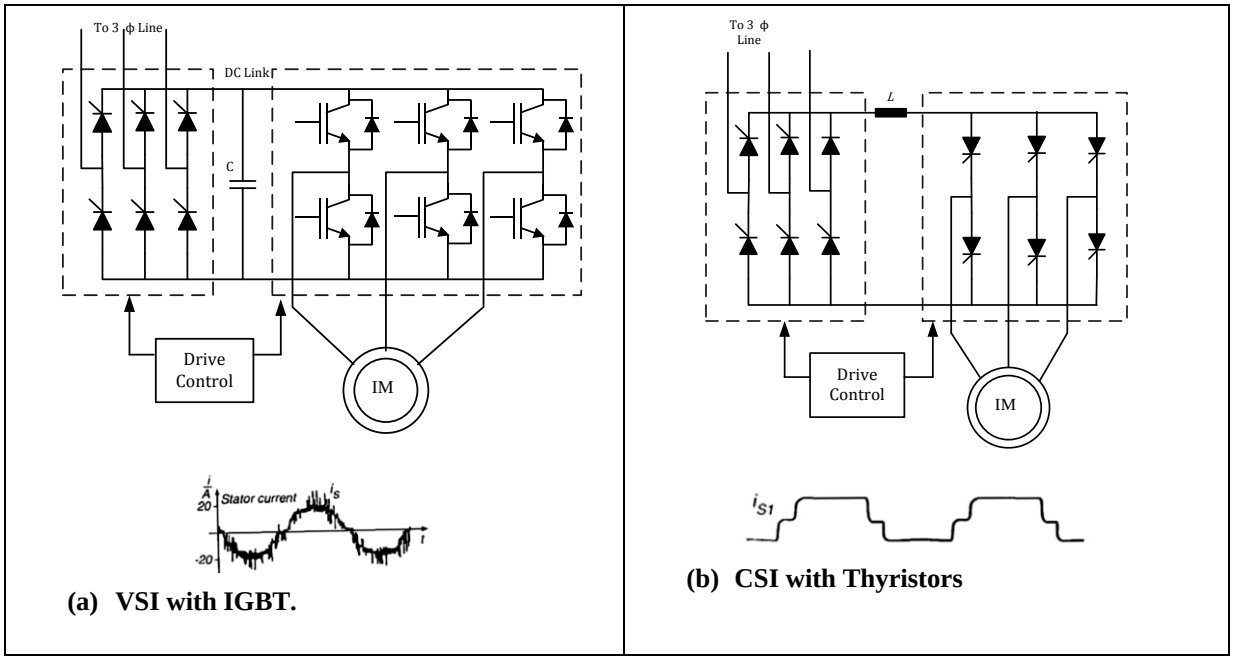


**Figure 2-1 : Four Quadrant Drives for the MV and High Power Applications.**

## 2.2. Vector Control of Three Phase Induction Motor.

### *2.2.1 Space Vectors.*

The Vector control or the high performance control allows the Induction motor to be controlled as the DC motor i.e. the torque and speed can be controlled independently; this control is also known as decoupled control, transvector control, or high performance control.

The theory of space vector forms the basis of the vector control; this theory was first developed for the multi-phase AC in Hungary. The space vectors in relation with the electrical machines can be viewed as the resultant of time varying quantities in the space.

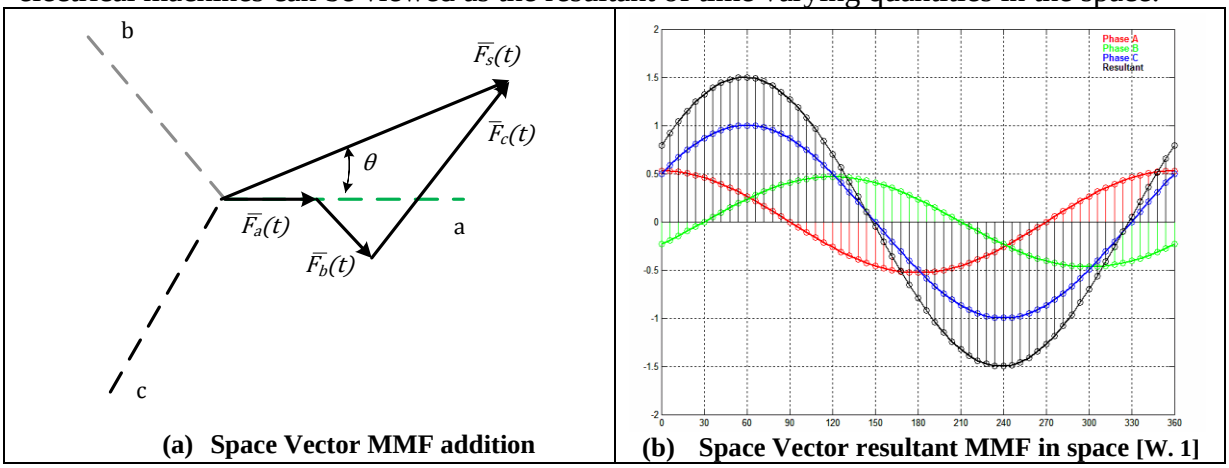


**(a) Space Vector MMF addition** **(b) Space Vector resultant MMF in space [W. 1]**

**Figure 2-2 : Space Vector representation.**

The three phase symmetrically spaced windings when fed with the balanced three phase sinusoidal currents produces the rotating magnetic field in the air gap. The resultant mmf in the space rotates at synchronous speed. This resultant mmf at any angle θ, at any time t along the stator periphery can be mathematically calculated as vector addition of the time varying currents.

$$\underline{f_s}(\theta,t) = N_{se}\left[i_{sa}(t)cos(\theta) + i_{sb}(t)\,cos\left(\theta - \frac{2\pi}{3}\right) + i_{sc}(t)cos\left(\theta - \frac{4\pi}{3}\right)\right] \quad \textbf{(2-1)}$$

Where $N_{se}$ is the effective number of stator turns including the winding and pitch factors. Similar to the mmf space vector the equations for the current and voltage space vector can be written, which proves very useful although both do not have any physical existence. Using Euler's identity the equation (2-1) can be re written as

$$\underline{f_s}(\theta,t) = \frac{1}{2}N_{se}\,Re\{\underline{I_S}(t)e^{-j\theta} + \underline{I_S^*}(t)e^{-j\theta}\} \quad \textbf{(2-2)}$$

$\underline{I_s}(t)$ is stator current space vector and $\underline{I_S^*}$ is complex conjugate of the same, the stator current space vector can be expressed as.

$$\underline{I_s}(t) = k\left[i_{sa}(t)e^{-j0} + i_{sb}(t)e^{-j\frac{2\pi}{3}} + i_{sc}(t)e^{-j\frac{4\pi}{3}}\right] \quad \textbf{(2-3)}$$

Where k is constant, if selected 2/3 and there are no zero sequence currents, then the projection of the space vector $\underline{I_s}(t)$ on the corresponding three phase axes will result instantaneous values of the respective phases.

### *2.2.2 Clark and Park Transforms.*

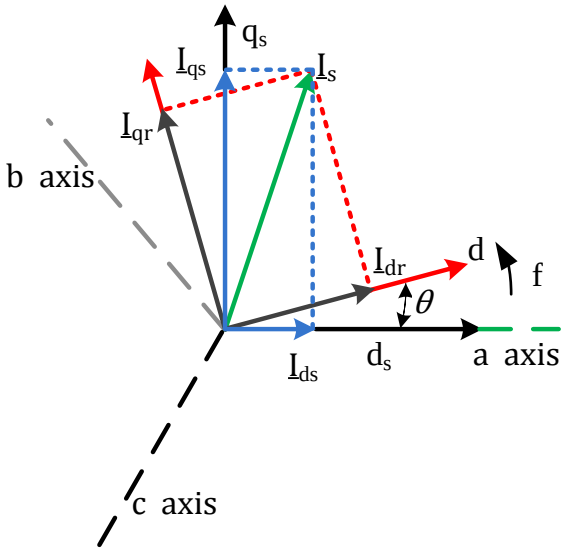


**Figure 2-3 : Clark and Park transformations for three phases.**

The Clarke transformations transform the three phase alternating quantities to two dimensional stationary reference frame.

$$\left[f^{s}{}_{dq0}\right] = \left[T^{s}{}_{dq0}\right][f_{abc}] \quad \textbf{(2-4)}$$

Where $\left[T^{s}{}_{dq0}\right]$ is the transformation matrix given by

$$\left[T^{s}{}_{dq0}\right] = \frac{2}{3}\begin{bmatrix} 1 & -\frac{1}{2} & -\frac{1}{2} \\ 0 & \sqrt{\frac{3}{2}} & -\sqrt{\frac{3}{2}} \\ \frac{1}{2} & \frac{1}{2} & \frac{1}{2} \end{bmatrix} \quad \textbf{(2-5)}$$

If the three phase system is balanced the last row of the equation (2-5) becomes zero and system is reduced to two variables d-q. When the Clark's transforms are further transformed using Parks transformations using equation (2-6) the stationary d-q-0 components are transformed to the rotating d-q-0 transforms.

$$\left[f^{r}{}_{dq}\right] = \left[T^{r}{}_{dq}\right]\left[f^{s}{}_{dq}\right] \tag{2-6}$$

Where $\left[T^{r}{}_{dq}\right]$ is the transformation matrix given by.

$$\left[T^{r}{}_{dq}\right] = \frac{2}{3}\begin{bmatrix} \cos\theta & \sin\theta \\ -\sin\theta & \cos\theta \end{bmatrix} \tag{2-7}$$

## 2.3. Equivalent circuit of three phase Induction Motor.

Vector control of induction motor requires the estimation of the flux in the machine. The calculation of the flux depends on the physical parameters of the machine hence it is required to represent the physical parameters of the machine such as resistances and inductances in equivalent circuit so that necessary mathematical equations can be set up for the flux estimation.

Induction machine can be represented with three different equivalent circuits, T equivalent, Γ equivalent and inverse Γ equivalent. Each one requires different numbers of parameters to describe the induction motor, such as T equivalent requires two resistances and three inductances, while Γ and inverse Γ requires two resistances and inductances to model the Induction Machine. These equivalent circuits are chosen for the control depending choice of the reference frame and availability of the motor parameters.

The T equivalent circuit is hardly used for the vector control of induction machine; it can be used when the air gap flux orientation is used. Γ and inverse Γ equivalent circuits are more commonly used. In the Γ equivalent circuit the total leakage impedance is transferred to the rotor side, this equivalent circuit is used while employing the stator oriented control. In inverse Γ equivalent circuit the total leakage impedance is transferred to the stator side, and it is used in rotor flux oriented control. Only four parameters are needed in all to model the induction motor in Γ and inverse Γ equivalent circuits i.e. two resistance and two inductances. Figure 2-4 summarizes the equivalent circuits for the induction motor and relevant equations used in each. The equations are written in d-q frame of reference rotating with the frequency f and all the values are in per unit.

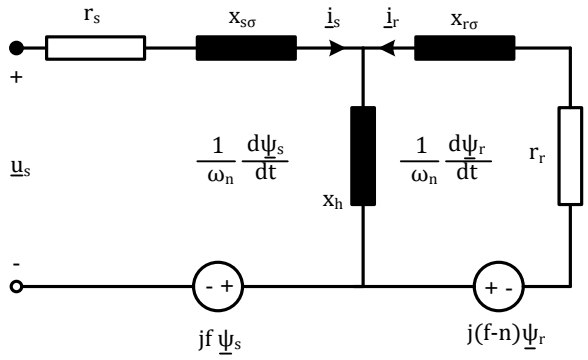


**(a) T equivalent circuit**

$$\underline{u_s} = r_s\underline{i_s} + \frac{1}{\omega_n}\frac{d\underline{\psi_s}}{dt} + jf\underline{\psi_s}$$

$$0 = r_r\underline{i_r} + \frac{1}{\omega_n}\frac{d\underline{\psi_r}}{dt} + j(f-n)\underline{\psi_r}$$

$$\underline{\psi_s} = x_s\underline{i_s} + x_h\underline{i_r}$$
$$\underline{\psi_r} = x_h\underline{i_s} + x_r\underline{i_r}$$

$$x_s = x_{s\sigma} + x_h = (1+\sigma_s)x_h$$
$$x_r = x_{r\sigma} + x_h = (1+\sigma_r)x_h$$
$$\sigma = 1 - \frac{1}{(1+\sigma_s)(1+\sigma_r)}$$

$$m_e = \frac{1}{(1+\sigma_r)}\left(\underline{\psi_{rd}}\underline{i_{sq}} - \underline{\psi_{rq}}\underline{i_{sd}}\right)$$

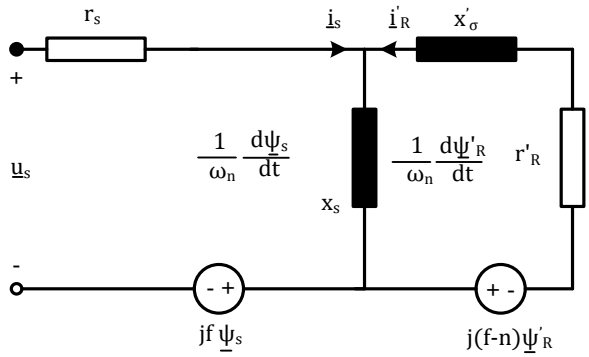


**(b) Γ equivalent circuit.**

$$\underline{u_s} = r_s\underline{i_s} + \frac{1}{\omega_n}\frac{d\underline{\psi_s}}{dt} + jf\underline{\psi_s}$$
$$0 = r_r\underline{i_R} + \frac{1}{\omega_n}\frac{d\underline{\psi'_R}}{dt} + j(f-n)\underline{\psi'_R}$$

$$\underline{\psi_s} = x_s\underline{i_s} + x_m\underline{i'_R}$$
$$\underline{\psi'_R} = x_s\underline{i_s} + (x_s + x'_\sigma)\underline{i'_R}$$

$$m_e = (1-\sigma)\left(\underline{\psi'}_{Rd}\underline{i_{sq}} - \underline{\psi'}_{Rq}\underline{i_{sd}}\right)$$

$$\underline{\psi'_R} = (1+\sigma_s)\underline{\psi_r}$$
$$\underline{i'_R} = \frac{\underline{i_r}}{1+\sigma_s}$$
$$x'_\sigma = \frac{\sigma}{1-\sigma}x_s$$
$$r'_R = (1+\sigma_s)^2 r_r$$

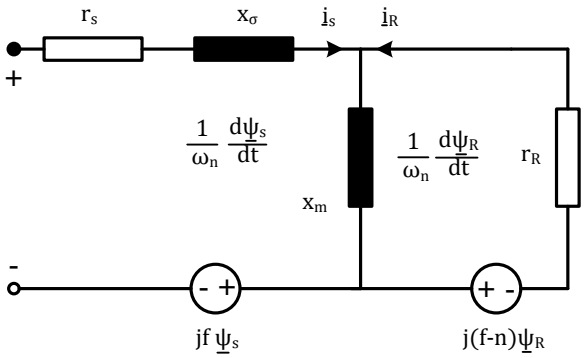


**(c) Inverse Γ equivalent circuit.**

$$\underline{u_s} = r_s\underline{i_s} + \frac{1}{\omega_n}\frac{d\underline{\psi_s}}{dt} + jf\underline{\psi_s}$$
$$0 = r_r\underline{i_R} + \frac{1}{\omega_n}\frac{d\underline{\psi_R}}{dt} + j(f-n)\underline{\psi_R}$$

$$\underline{\psi_s} = (x_m + x_\sigma)\underline{i_s} + x_m\underline{i_R}$$
$$\underline{\psi'_R} = x_m(\underline{i_s} + \underline{i_R})$$

$$m_e = \left(\underline{\psi_{Rd}}\underline{i_{sq}} - \underline{\psi_{Rq}}\underline{i_{sd}}\right)$$

$$\underline{\psi_R} = \frac{\underline{\psi_r}}{(1+\sigma_r)}$$
$$\underline{i_R} = \underline{i_r}(1+\sigma_r)$$
$$x_\sigma = \sigma x_s \qquad x_m = \frac{x_h}{(1+\sigma_r)}$$
$$r_R = \frac{r_r}{(1+\sigma_r)^2}$$

**Figure 2-4 : Equivalent circuits of three phase Induction motor.**

## 2.4. Indirect Vector Control of the Induction Machine and Flux Estimators.

Various methods for the Vector control of the induction machine evolved over the period of time, the methods are described in brief in [B.1], since the indirect vector control method is used in the thesis, it is relevant to present the brief overview of the same along with the flux estimators that will be used in the drive.

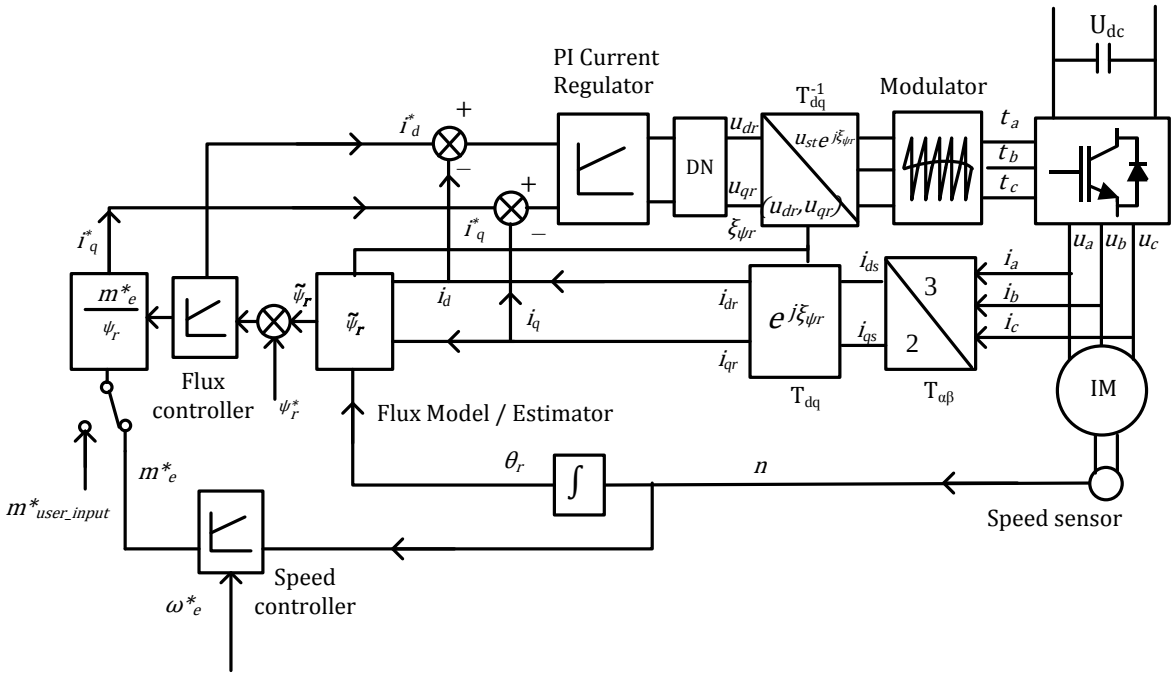


**Figure 2-5 : Indirect vector control of three phase Induction motor.**

The indirect or the feed forward vector control method employs a speed sensor, usually an incremental encoder. The speed signal form encoder is used to generate the rotor angle which is then added to the slip angle calculated from the flux model to determine the instantaneous angle of the rotor flux $\xi_{\psi r}$. The rotor flux rotates in the air gap with the synchronous speed. The rotor flux vector angle $\xi_{\psi r}$ is used to transform the stationary $d_s$-$q_s$ components of currents to the synchronously rotating $d_r$-$q_r$ reference frame.

The flux model estimates the flux and the instantaneous flux position in the machine. Estimated flux is compared with the reference and regulated by PI regulator to generate the direct axis current reference. The q axis current component is either generated by the speed controller or the user defined torque input. The reference currents $i^*_d$ and $i^*_q$ are compared with the transformed $d_r$-$q_r$ currents and regulated by the PI controllers to generates the reference voltages $u_d$ and $u_q$. The voltage reference signals then transformed back to the three phases and are fed to the modulator to produce the switching sequences for the PPU.

The rotor flux is always kept constant and aligned to the direct axis with help of the coordinate transformations so that there is no q axis flux linkage and thus the decoupled control or the high performance of the induction motor is possible.

The rotor flux estimator or the flux model is very important in the vector control of the induction machine. The most simple and commonly used flux estimator is current model. It gives very good results in the in general, the only drawback is that the flux estimation accuracy depends upon the rotor time constant, which changes as the temperature of the rotor varies. This leads to the incorrect estimation of the flux magnitude as well as position which results in poor dynamic response.
Using the stator and rotor voltage equations in the inverse Γ equivalent circuit the following equations can be derived for the flux and instantaneous angular position in the synchronously rotating d-q reference frame.

$$\frac{d\underline{\tilde{\psi}}_R}{dt} = \frac{\underline{\tilde{\psi}}_R}{T_r} + \frac{x_R}{T_r}\,\underline{\tilde{\imath}}_{sd}$$

$$\frac{d\tilde{\xi}_R}{dt} = \omega_n\left(f_{\psi_r} + n\right) = \omega_n\left(\frac{x_m \cdot \underline{\tilde{\imath}}_{sd}}{T_r \cdot \underline{\tilde{\psi}}_R} + n\right)$$

**(2-8)**

Voltage model using the stator currents in the stationary α-β components and the stator resistance can be used to determine the flux estimation. This is provides more accurate estimate of the rotor flux vector in the high speed range. The rotor flux can be estimated using the stator voltage equations as shown below.

$$\underline{\tilde{\psi}}_{ds} = \int(\underline{u}_{ds} - \underline{\tilde{\imath}}_{ds} r_s)dt$$

$$\underline{\tilde{\psi}}_{qs} = \int(\underline{u}_{qs} - \underline{\tilde{\imath}}_{qs} r_s)dt$$

**(2-9)**

From the flux linkage equations in the inverse Γ equivalent circuit as shown in the Figure 2-4, if the rotor currents are eliminated, the rotor flux linkage equations in stationary α-β coordinate can be written as below.

$$\underline{\tilde{\psi}}_{dr} = (1 + \sigma_r)\left(\underline{\tilde{\psi}}_{ds} - x_\sigma \cdot \underline{\tilde{\imath}}_{ds}\right)$$
$$\underline{\tilde{\psi}}_{qr} = (1 + \sigma_r)\left(\underline{\tilde{\psi}}_{qs} - x_\sigma \cdot \underline{\tilde{\imath}}_{qs}\right)$$

**(2-10)**

This estimator is mostly used in the stator oriented control. This flux model in the low speed range introduces serious errors due to open integration as the stator voltages are very low. More ever if the stator resistance estimate contains error the flux estimation is erroneous, resulting poor dynamic response.

# 3. Modelling of Six Phase Induction Machines.

Multi-phase machines are of two types, symmetrical and asymmetrical. When the windings of the multi-phase machine are wound such that the spatial displacement between the axes of two phase groups is $\frac{2\pi}{n}$,where n is total number of phases then the machine is said to be symmetrical, otherwise it is asymmetrical. The machine used in the thesis is six phase asymmetrical squirrel cage induction motor with $\frac{\pi}{6}$ phase displacement between the axes of two phase groups.

## 3.1. Vector space decomposition.

Six phase induction machine as shown schematically in the
Figure 3-1 is a six dimensional system of phasors i.e. current and voltages. For simplifying modeling and control of the six phase machine it is required to transform these six dimensional system of phasors into the another six orthogonal axes. These axes can be found by using the base vectors [8].Using this base vector the existing set of the six phase voltages can be transformed to new set of axes which are mutually perpendicular. The base vector matrix is as below.

$$\mathrm{T} = \frac{1}{3}\begin{bmatrix} 1 & cos(\theta) & cos(4\theta) & cos(5\theta) & cos(8\theta) & cos(9\theta) \\ 0 & sin(\theta) & sin(4\theta) & sin(5\theta) & sin(8\theta) & sin(9\theta) \\ 1 & cos(5\theta) & cos(8\theta) & cos(\theta) & cos(4\theta) & cos(9\theta) \\ 0 & sin(5\theta) & sin(8\theta) & sin(\theta) & sin(4\theta) & sin(9\theta) \\ 1 & 0 & 1 & 0 & 1 & 0 \\ 0 & 1 & 0 & 1 & 0 & 1 \end{bmatrix} \quad \textbf{(3-1)}$$

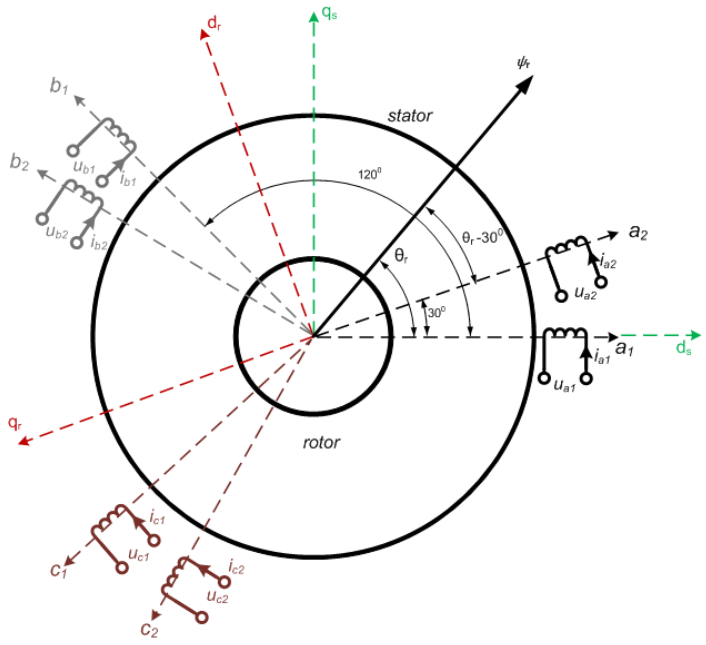


**Figure 3-1: Six Phase Induction Machine.**

The actual transformation matrix from the six phase quantities to the d-q-z subspace can be written by putting $\theta = \frac{\pi}{6}$ in equation (3-1, which is angle between the two phase groups

$$T = \frac{1}{3}\begin{bmatrix} 1 & \frac{\sqrt{3}}{2} & -\frac{1}{2} & -\frac{\sqrt{3}}{2} & -\frac{1}{2} & 0 \\ 0 & \frac{1}{2} & \frac{\sqrt{3}}{2} & \frac{1}{2} & -\frac{\sqrt{3}}{2} & -1 \\ 1 & -\frac{\sqrt{3}}{2} & -\frac{1}{2} & \frac{\sqrt{3}}{2} & -\frac{1}{2} & 0 \\ 0 & \frac{1}{2} & -\frac{\sqrt{3}}{2} & \frac{1}{2} & \frac{\sqrt{3}}{2} & -1 \\ 1 & 0 & 1 & 0 & 1 & 0 \\ 0 & 1 & 0 & 1 & 0 & 1 \end{bmatrix} \quad \textbf{(3-2)}$$

This transformation is also termed as the vector space decomposition [8]. This is similar as stationary d-q-0 transformations in the case of three phase machines however in six phase machine additional set of axes are present and are termed as $z_1$-$z_2$ axes. If the neutrals of the two phase groups are isolated there are no zero sequence currents in the system, the transformations in Equation (3-2) has following important features [8].

- The fundamental components of machine currents along with the $k^{th}$ order harmonics with k=12m+ 1 (m =1, 2, 3….) are transformed into the d-q subspaces.
- All the harmonics with k= 6m+ 1 are transformed into the z1-z2 subspaces.
- All the zero sequence harmonics (m-3) are transformed into the 01-02 subspaces

### 3.2. Electromagnetic system.

Before proceeding further it is important to mention assumptions that are made while modelling.

1. Capacitances of windings are neglected.
2. Each distributed winding is represented as a concentrated winding producing sinusoidal flux distribution in air gap.
3. Magnetic saturation is neglected.

The model of the six phase machine is based on the model presented in [8]

In six phase induction machine there are six voltage equations in stator and one for the rotor, for the physical model the equations can be written in the matrix form as below.

$$\underline{\boldsymbol{U}}_{\boldsymbol{SR}} = \boldsymbol{R}_{\boldsymbol{SR}} \cdot \underline{\boldsymbol{I}}_{\boldsymbol{SR}} + \frac{d\underline{\boldsymbol{\Psi}}_{\boldsymbol{SR}}}{dt} \quad \textbf{(3-3)}$$

The flux is given as

$$\underline{\boldsymbol{\Psi}}_{\boldsymbol{SR}} = \boldsymbol{X}_{\boldsymbol{SR}}.\underline{\boldsymbol{I}}_{\boldsymbol{SR}} \tag{3-4}$$

The voltage, current and flux linkage matrices are listed in the appendix.

### 3.3. Mechanical system.

The mechanical system can be described using the Newton's law of motion for the rotational system as shown below.

$$J\frac{d\Omega}{dt} = M_e - M_L$$

$$\frac{d\theta_{mech}}{dt} = \Omega$$

$$\theta = p.\theta_{mech} \tag{3-5}$$

The torque $M_e$ can be expressed as

$$M_e = \frac{1}{2}(I^{SR})^T.\frac{\partial X^{SR}}{\partial \theta_{mech}}.\underline{I}^{SR} = \frac{p}{2}.(I^{SR})^T.\frac{\partial X^{SR}}{\partial \theta}.\underline{I}^{SR} \tag{3-6}$$

### 3.4. Transformation of co-ordinates.

Using equation (3-2)vector space of the SPIM can be decomposed to the d-q, $z_1$-$z_2$ , $0_1$-$0_2$ subspaces. The stator and rotor equations can be written in stationary reference frame, as shown in

Figure 3-1.Thus the voltage equation (3-3) for the machine can be transformed as below.

$$\boldsymbol{T}.\underline{U}^S = \boldsymbol{T}.R^S.\boldsymbol{T^{-1}}.\boldsymbol{T}.\underline{I}^S + \boldsymbol{T}\frac{d(\boldsymbol{T^{-1}}\underline{\Psi}^{SR})}{dt} \tag{3-7}$$

The equation (3-7) can be written for decomposed subspaces as below.

**d-q subspace**

Stator voltage equation.

$$\begin{bmatrix} U^s_{sd} \\ U^s_{sq} \end{bmatrix} = \begin{bmatrix} R_s & 0 \\ 0 & R_s \end{bmatrix}.\begin{bmatrix} I^s_{sd} \\ I^s_{sq} \end{bmatrix} + \frac{d}{dt}\left\{\begin{bmatrix} X_{s\sigma}+X_h & 0 \\ 0 & X_{s\sigma}+X_h \end{bmatrix}.\begin{bmatrix} I^s_{sd} \\ I^s_{sq} \end{bmatrix} + L_h.\begin{bmatrix} cos\,\theta_r & -sin\,\theta_r \\ sin\,\theta_r & cos\,\theta_r \end{bmatrix}.\begin{bmatrix} I^r_{sd} \\ I^r_{sq} \end{bmatrix}\right\} \tag{3-8}$$

Rotor voltage equation.

$$\begin{bmatrix}0\\0\end{bmatrix} = \begin{bmatrix}R_r & 0\\0 & R_r\end{bmatrix}.\begin{bmatrix}I_{sd}^r\\I_{sq}^r\end{bmatrix} + \frac{d}{dt}\left\{\begin{bmatrix}X_{r\sigma}+X_h & 0\\0 & X_{r\sigma}+X_h\end{bmatrix}.\begin{bmatrix}I_{sd}^r\\I_{sq}^r\end{bmatrix} + L_h.\begin{bmatrix}cos\,\theta_r & -sin\,\theta_r\\sin\,\theta_r & cos\,\theta_r\end{bmatrix}.\begin{bmatrix}I_{sd}^s\\I_{sq}^s\end{bmatrix}\right\} \quad \textbf{(3-9)}$$

**$z_1$-$z_2$ subspace**

**Stator equation** **Rotor equation**

$$\begin{bmatrix}U_{z_1}^s\\U_{z_2}^s\end{bmatrix} = \begin{bmatrix}R_s+\frac{d}{dt}X_{s\sigma} & 0\\0 & R_s+\frac{d}{dt}X_{s\sigma}\end{bmatrix}.\begin{bmatrix}I_{z_1}^s\\I_{z_2}^s\end{bmatrix} \qquad \begin{bmatrix}0\\0\end{bmatrix} = \begin{bmatrix}R_r+\frac{d}{dt}X_{r\sigma} & 0\\0 & R_r+\frac{d}{dt}X_{r\sigma}\end{bmatrix}.\begin{bmatrix}I_{z_1}^r\\I_{z_2}^r\end{bmatrix}$$

**(3-10)**

**Stator equation** **Rotor Equation**

$$\begin{bmatrix}U_{0_1}^s\\U_{0_2}^s\end{bmatrix} = \begin{bmatrix}R_s+\frac{d}{dt}X_{s\sigma} & 0\\0 & R_s+\frac{d}{dt}X_{s\sigma}\end{bmatrix}.\begin{bmatrix}I_{0_1}^s\\I_{0_2}^s\end{bmatrix} \qquad \begin{bmatrix}0\\0\end{bmatrix} = \begin{bmatrix}R_r+\frac{d}{dt}X_{r\sigma} & 0\\0 & R_r+\frac{d}{dt}X_{r\sigma}\end{bmatrix}.\begin{bmatrix}I_{0_1}^r\\I_{0_2}^r\end{bmatrix}$$

**(3-11)**

To eliminate the position dependent inductance in the rotor equations it is necessary to refer the rotor equation with the same reference frame as that of stator for that following simple transforms serves the purpose. The inductance matrix after transformation can be found in appendix

$$T_r^s = \begin{bmatrix}cos(\theta_r) & -sin(\theta_r)\\sin(\theta_r) & cos(\theta_r)\end{bmatrix} \quad \textbf{(3-12)}$$

The torque can be written as

$$M_e = \frac{p}{2}.(I^{SR})^T.\frac{\partial X^{SR}}{\partial\theta}.\underline{I}^{SR} = \frac{p}{2}.\left(\boldsymbol{T^{-1}}.\underline{I}^r\right)^T.\frac{\partial X^{SR}}{\partial\theta}.\boldsymbol{T^{-1}}.\underline{I}^r = \frac{p}{2}.(I^r)^T.(\boldsymbol{T^{-1}})^T.\frac{\partial X^{SR}}{\partial\theta}.\boldsymbol{T^{-1}}.\underline{I}^r$$

This can be written as

$$M_e = 3.p.\left(\underline{I}^r\right)^T.\underline{\Psi}^r = 3.p.(\Psi_d.I_q - \Psi_q.I_d) \quad \textbf{(3-13)}$$

### 3.5. Per unit system

Average power input to the machine over a fundamental period is generally the basis of the power in AC system, the input power is given as

$$P_{sN} = 6.\frac{\hat{U}_{phN}.\hat{I}_{phN}}{2}.\cos\phi_N = 6.U_{phN,rms}.I_{phN,rms}.\cos\phi_N$$

**(3-14)**

Writing in terms of apparent power

$$S_N = 6.\frac{\hat{U}_{phN}.\hat{I}_{phN}}{2} = 3.\hat{U}_{phN}.\hat{I}_{phN} = 6.U_{phN,rms}.I_{phN,rms} = 2.\sqrt{3}.U_N.I_N$$

**(3-15)**

Here $U_N$ and $I_N$ are the rms values of the line voltage and line currents respectively from the above equation it is evident that for the same voltage rating the current per phase of the SPIM is halved as compared with the same rating of three phase IM.

For six windings 6 basis voltages and currents are to be chosen while scaling the model, so for that rated per phase peak values are used as the base values in the stator windings.

$$I_{dn} = I_{qn} = I_{z1n} = I_{z2n} = I_{01n} = I_{02n} = \hat{I}_N$$

$$U_{dn} = U_{qn} = U_{z1n} = U_{z2n} = U_{01n} = U_{02n} = \hat{U}_{phN}$$

$$\Psi_{dn} = \Psi_{qn} = \Psi_{z1n} = \Psi_{z2n} = \Psi_{01n} = \Psi_{02n} = \Psi_N = \frac{\hat{U}_{phN}}{\omega_n} = \frac{\hat{U}_{phN}}{2.\pi.f_n}$$

**(3-16)**

It can be seen that the product of current and voltage in each winding becomes equal to the base for the power.

The scaling of power for the stator then becomes.

$$P_S = 3.\left(U_d.I_d + U_q.I_q + U_{z1}.I_{dz1} + U_{z2}.I_{z2} + U_{01}.I_{01} + U_{02}.I_{02}\right)$$

$$S_N = 3.\left(\hat{U}_{phN}.\hat{I}_{phN}\right)$$

$$\wp = \frac{P_S}{S_N} = 3.\left(u_d.i_d + u_q.i_q + u_{z1}.i_{dz1} + u_{z2}.i_{z2} + u_{01}.i_{01} + u_{02}.i_{02}\right)$$

**(3-17)**

The base torque at the synchronous speed $\Omega_N$ can be written as below.

$$M_n = \frac{S_N}{\Omega_N} = p.\frac{S_N}{\omega_n} = 3.p.\frac{\hat{U}_{phN}.\hat{I}_{phN}}{\omega_n} = 3.p.\hat{\Psi}_n.\hat{I}_{phN}$$

The per unit torque can be written as

$$m_e = \frac{M_e}{M_n} = \frac{3.p.(\Psi_d.I_q - \Psi_q.I_d)}{3.p.\hat{\Psi}_n.\hat{I}_{phN}} = \psi_d.I_q - \psi_q.I_d$$

**(3-18)**

The mechanical time constant is

$$T_m = \frac{J.\Omega^2_N}{S_N}$$

The model for the mechanical system can be written as

$$T_m\frac{dn}{dt} = m_e - m_L \qquad \frac{d\theta}{dt} = \omega_n.n \qquad \theta_{mech} = \frac{\theta}{p}$$

**(3-19)**

### 3.6. Transformed Model of SPIM

After the transformations and introduction of the per unit system the equations for the SPIM for the stator and rotor can be written as below. Note that here the d-q axis is fixed in stator as shown in

Figure 3-1.

| **Subspace** | **Stator** | **Rotor** |
|---|---|---|
| $d-q$ | $u_{sd} = r_s.i_{sd} + \frac{1}{\omega_n}\frac{d\psi_{sd}}{dt}$ | $0 = r_r.i_{rd} + \frac{1}{\omega_n}\frac{d\psi_{rd}}{dt} - n.\psi_{rq}$ |
| | $u_{sq} = r_s.i_{sq} + \frac{1}{\omega_n}\frac{d\psi_{sq}}{dt}$ | $0 = r_r.i_{rq} + \frac{1}{\omega_n}\frac{d\psi_{rq}}{dt} + n.\psi_{rd}$ |
| $z_1-z_2$ | $u_{z1} = r_s.i_{z1} + \frac{1}{\omega_n}\frac{d\psi_{z1}}{dt}$ | $0 = r_r.i_{z1} + \frac{1}{\omega_n}\frac{d\psi_{z1}}{dt}$ |
| | $u_{z2} = r_s.i_{z2} + \frac{1}{\omega_n}\frac{d\psi_{z2}}{dt}$ | $0 = r_r.i_{z2} + \frac{1}{\omega_n}\frac{d\psi_{z2}}{dt}$ |
| $0_1-0_2$ | $u_{01} = r_s.i_{01} + \frac{1}{\omega_n}\frac{d\psi_{01}}{dt}$ | $0 = r_r.i_{01} + \frac{1}{\omega_n}\frac{d\psi_{01}}{dt}$ |
| | $u_{02} = r_s.i_{02} + \frac{1}{\omega_n}\frac{d\psi_{02}}{dt}$ | $0 = r_r.i_{02} + \frac{1}{\omega_n}\frac{d\psi_{02}}{dt}$ |

**(3-20)**

Here the mutual leakage inductances in the stator are neglected.

The flux linkage equations are as below.

| **Subspace** | **Stator** | **Rotor** |
|---|---|---|
| $d-q$ | $\psi_{sd} = x_s.i_{sd} + x_h.i_{rd}$ | $\psi_{rd} = x_r.i_{rd} + x_h.i_{sd}$ |
| | $\psi_{sq} = x_s.i_{sq} + x_h.i_{rq}$ | $\psi_{rq} = x_r.i_{rq} + x_h.i_{sq}$ |
| $z1-z2$ | $\psi_{sz1} = x_{s\sigma}.i_{sz1}$ | $\psi_{rz1} = x_{r\sigma}.i_{rz1} = 0$ |
| | $\psi_{sz2} = x_{s\sigma}.i_{sz2}$ | $\psi_{rz2} = x_{r\sigma}.i_{rz2} = 0$ |
| $01-02$ | $\psi_{s01} = x_{s\sigma}.i_{s01}$ | $\psi_{r01} = x_{r\sigma}.i_{r01} = 0$ |
| | $\psi_{s02} = x_{s\sigma}.i_{s02}$ | $\psi_{r02} = x_{r\sigma}.i_{r02} = 0$ |

**(3-21)**

Reactances are as below

$$x_s = x_{s\sigma} + x_h \qquad x_r = x_{r\sigma} + x_h$$

**(3-22)**

And finally the mechanical system

$$T_m \frac{dn}{dt} = m_e - m_L \qquad \frac{d\theta}{dt} = \omega_n.n \qquad \theta_{mech} = \frac{\theta}{p}$$

**(3-23)**

For the $z_1$-$z_2$ and $0_1$-$0_2$ subspace for the rotor equations it can be seen that there is no excitation in the rotor circuit, this means that this do not contribute to the machine dynamics. Also the flux linkage variation in the rotor z and 0 subspaces is zero. So the rotor dynamics for the z and zero subspace will be neglected.

# 4. Control Schemes for Six Phase Induction Machine.

The control of the SPIM involves the location of the control voltage vector in six dimensional subspaces such that it will produce the desired magnetization for motor and deliver the required torque. Detail analysis and comparative study of various modulation techniques are discussed in [10] for the control of SPIM, relevant few are discussed briefly in the next subsection.

## 4.1. Conventional SVM technique.

For the six leg two level inverter there are $2^6 = 64$ switching states as shown in the [8] in Figure 4-1. This method was proposed in [8], this is called conventional SVM as it is same that is being used in the three phase drives. Two adjacent space vectors and one zero vector are used to calculate the desired reference vector as shown in the Figure 4-1(a), since only three vectors are used out of five, it results in generation of harmonic voltage in the $z_1$-$z_2$ subspace resulting the extra losses.

## 4.2. Vector space decomposition technique.

This method was also first proposed in [8], which uses four adjacent voltage vectors and one zero vector to calculate the reference vector as shown in Figure 4-1(b). This method minimizes the harmonics in the $z_1$-$z_2$ subspaces, however this method is more complicated to implement than previous and it requires more computational power which may increase the cost of the drive.

## 4.3. Vector classification technique.

This method is quite different as compared to the previous two mentioned above, the previous two methods employs single unit of six legged two level inverter to drive the SPIM while this one uses two three legged two level inverter. This method is discussed in [11]

In this method two three legged two level inverters are controlled independently and the switching state vectors are mapped into the inverter basis frame rather than machine basis frame as shown in the Figure 4-1(c).

This method can be implemented in two ways, in the first the same reference vector is applied to the modulators with one modulator switching states having phase shift of $30^0$ with respect to the other refer Figure 4-1(c).

In second method two reference vectors are used which are $30^0$ phase shifted with respect to one another to control the inverters having the same switching states, this method will be implemented in the control of SPIM with split dc link.

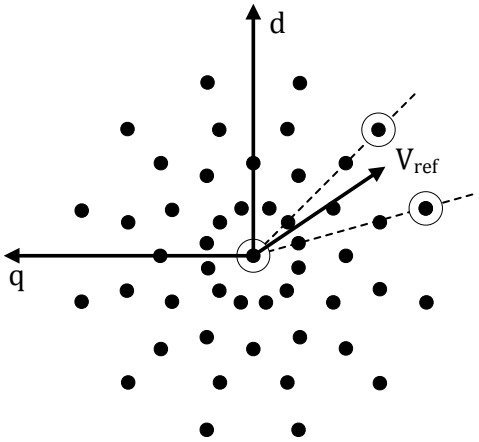


**(a). Conventional SVM technique.**

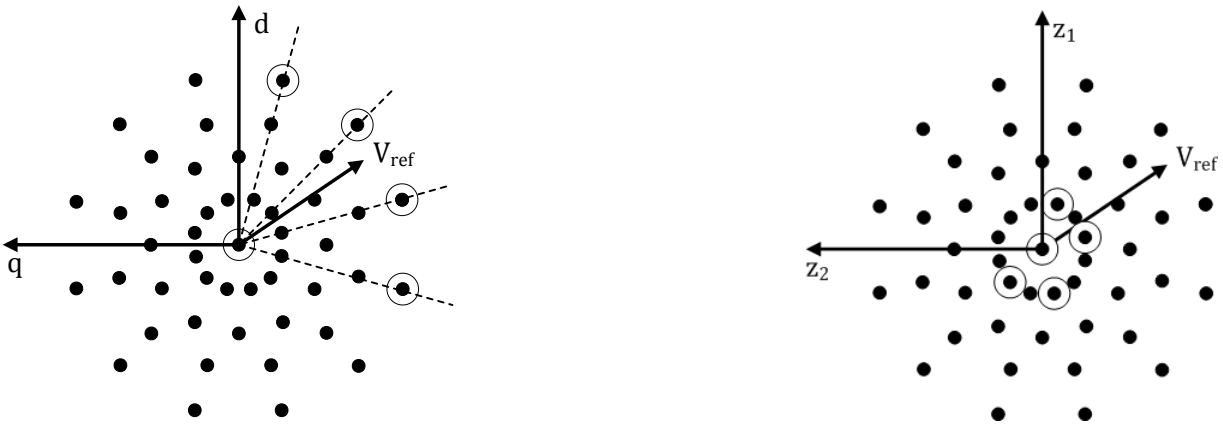


**(b). Vector space decomposition.**

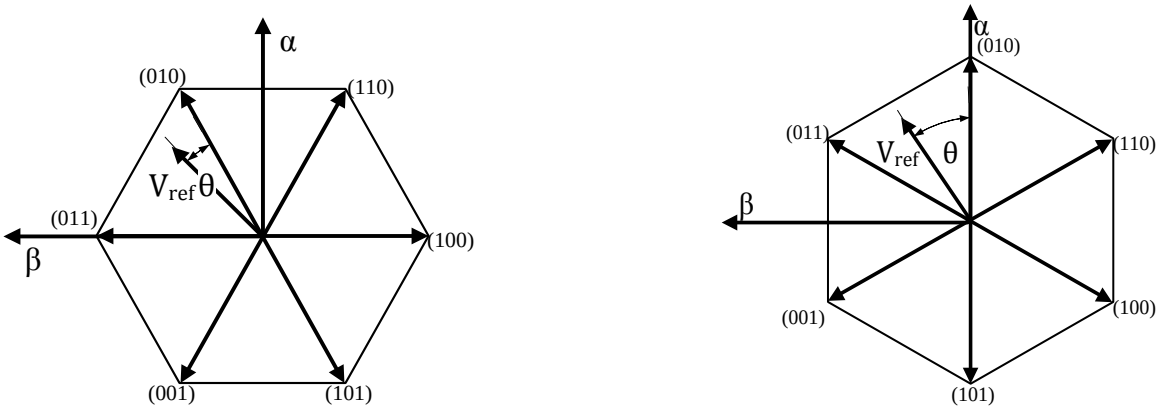


**(c). Vector classification technique.**
**Figure 4-1. Different modulation techniques for SPIM. [10]**

The advantages this method offer is that the control is simple than the previous two, since two three phase inverters are to be controlled independently, so no extra computational capabilities are needed for the signal processors. Thus one can use the existing two three phase modules of inverter and reprogram the DSP or FPGA to build the six phase drive.

However unlike the vector space decomposition technique this method does not directly control the excitation of the $z_1$-$z_2$ subspaces, but the harmonics in the phase currents are less as compared to the conventional space vector modulation technique.

Since the method similar to vector classification technique will be implemented with split DC link in SPIM drive, at this stage it is worthwhile to discuss the relationship between the voltage and current in motor d-q frame of reference to the individual d-q frame of references of the inverters.

For the individual inverters the phase voltages can be transformed to their own stationary d-q frame of reference using Clark transformations as below.

For inverter 1 it is assumed that the d-q frame of reference is aligned to the stator fixed d-q reference frame of SPIM.

$$\begin{bmatrix} U_{d1}^{s} \\ U_{q1}^{s} \\ U_{01}^{s} \end{bmatrix} = \frac{1}{3}\begin{bmatrix} 2 & -1 & -1 \\ 0 & \sqrt{3} & -\sqrt{3} \\ 1 & 1 & 1 \end{bmatrix}\begin{bmatrix} U_{a1} \\ U_{b1} \\ U_{c1} \end{bmatrix} \quad \textbf{(4-1)}$$

For the inverter 2 the transformations should be shifted at an angle $30^0$ in space as the second phase group is displaced $30^0$ in the space with respect to first as shown in the

Figure 3-1

$$\begin{bmatrix} U_{d2}^{s} \\ U_{q2}^{s} \\ U_{02}^{s} \end{bmatrix} = \frac{1}{3}\begin{bmatrix} \sqrt{3} & -\sqrt{3} & 0 \\ 1 & 1 & -2 \\ 1 & 1 & 1 \end{bmatrix}\begin{bmatrix} U_{a2} \\ U_{b2} \\ U_{c2} \end{bmatrix} \quad \textbf{(4-2)}$$

Comparing the above two equations with the equation (3-2) it can be seen that [15]

$$\begin{bmatrix} U_{d}^{s} \\ U_{q}^{s} \end{bmatrix} = \frac{1}{2}\left\{\begin{bmatrix} U_{d1}^{s} \\ U_{q1}^{s} \end{bmatrix} + \begin{bmatrix} U_{d2}^{s} \\ U_{q2}^{s} \end{bmatrix}\right\} \quad \textbf{(4-3)}$$

The same relationship holds true for the currents also.

# 5. Control schemes evaluated for six phase motor drive.

## 5.1. Double Synchronous Frame Current Control.

Figure 5-1 shows the block diagram of the DSFC control scheme that is implemented in the evaluation of the performance of FPGA based SPIM drive. This block diagram is based on the simulation and work carried out in [9] on the PMSM.

As shown in the figure the split DC link is used for the drive, with the two separate rectifiers supplying the power to the two inverters; the idea behind the use of the split DC link is to increases the redundancy of the drive system.

The six phase currents are first transformed using individual three phase Clark transforms, and then Park transforms are taken with $30^0$ phase shift to rotate the reference frame with the rotor flux vector, refer Figure 3-1. The two individual d-q currents are then transformed to the six phase d-q with the relationship mentioned in the equation (4-3). It was decided earlier to implement direct six phase transforms as proposed in the [21] ; however since the two three phase transforms makes code more flexible in case if it is to be used for the three phase machine , the idea of direct six phase transforms is rejected.

The flux model is essentially current model as discussed in the section 2.4, equation (2-8) I uses the rotor position from the pulse encoder to estimate the angle of the rotor flux vector.

Decoupling block processes these transformed currents and calculates the feed forward term for the two d-q controllers.

At this point it is required to mention how the decoupling will be achieved. From equation (4-3) it can be seen that the response in the motor d-q current will be same if there is step change in the d-q voltages of either of the inverter.

Splitting the d-q components of motor into d-q components of the different three phase groups and using three phase transformation for the individual three phase group in rotor reference frame, the d-q equations can be written as shown in (5-3) in control philosophy it is assumed that for inverter 1, $u_{d1}$ and $u_{q1}$ are used to control $i_{d1}$ and $i_{q1}$ and for the inverter 2, $u_{d2}$ and $u_{q2}$ are used to control $i_{d2}$ and $i_{q2}$.

For inverter 1 writing the d-q quantities, with d axis aligned to rotor flux linkage vector.[B.3]

$$\frac{di_{sd1}^{\Psi_r}}{dt} = -\frac{1}{T_s^{"}} i_{sd1}^{\Psi_r} + \omega_n . f_{\Psi_r} . i_{sq1}^{\Psi_r} - \frac{(1-\sigma)}{\sigma T_r} . \frac{\Psi_R}{x_H} + \frac{\omega_n}{x_\sigma} . u_{sd1}^{\Psi_r}$$

$$\frac{di_{sq1}^{\Psi_r}}{dt} = -\frac{1}{T_s^{"}} i_{sq1}^{\Psi_r} - \omega_n . f_{\Psi_r} . i_{sd1}^{\Psi_r} - \frac{(1-\sigma)}{\sigma x_H} . n . \Psi_R + \frac{\omega_n}{x_\sigma} . u_{sq1}^{\Psi_r} \quad \textbf{(5-1)}$$

Similarly for the inverter 2,

$$\frac{di_{sd2}^{\Psi_r}}{dt} = -\frac{1}{T_s^{"}} i_{sd2}^{\Psi_r} + \omega_n . f_{\Psi_r} . i_{sq2}^{\Psi_r} - \frac{(1-\sigma)}{\sigma T_r} . \frac{\Psi_R}{x_H} + \frac{\omega_n}{x_\sigma} . i_{sd2}^{\Psi_r}$$

$$\frac{di_{sq2}^{\Psi_r}}{dt} = -\frac{1}{T_s^{"}} i_{sq2}^{\Psi_r} - \omega_n . f_{\Psi_r} . i_{sd2}^{\Psi_r} - \frac{(1-\sigma)}{\sigma x_H} . n . \Psi_R + \frac{\omega_n}{x_\sigma} . u_{sq2}^{\Psi_r}$$

**(5-2)**

Where

$$T_s^{"} = \frac{x_\sigma}{\omega_n . r_s^{'}} \ , r_s^{'} = r_s + r_R \ , x_H = \frac{x_h}{1+\sigma_r} , r_R = \frac{r_r}{(1+\sigma_r)^2} , \Psi_R = \frac{\Psi_r}{1+\sigma_r} , \sigma = 1 - \frac{{x_h}^2}{x_s . x_r}$$

From the equations (5-1) and (5-2) the feed forward terms can be written as shown below.

$$u_{sdII}^{\Psi_r} = u_{sd1II}^{\Psi_r} + u_{sd2II}^{\Psi_r} = -\omega_n . f_{\Psi_r} . i_{sq1}^{\Psi_r} - \frac{(1-\sigma)}{\sigma T_r} . \frac{\Psi_R}{x_H} - \omega_n . f_{\Psi_r} . i_{sq1}^{\Psi_r} - \frac{(1-\sigma)}{\sigma T_r} . \frac{\Psi_R}{x_H}$$

$$= -\omega_n . f_{\Psi_r} . \left( i_{sq1}^{\Psi_r} + i_{sq2}^{\Psi_r} \right) - 2 . \frac{(1-\sigma)}{\sigma T_r} . \frac{\Psi_R}{x_H}$$

From the relationship of d-q parameters as shown in equation (4-3) which also true for the currents, above equation can be modified as

$$u_{sdII}^{\Psi_r} = u_{sd1II}^{\Psi_r} + u_{sd2II}^{\Psi_r} = -2 . (\omega_n . f_{\Psi_r} . i_{sq}^{\Psi_r} + \frac{(1-\sigma)}{\sigma T_r} . \frac{\Psi_R}{x_H})$$

Similarly for the q axis

$$u_{sqII}^{\Psi_r} = u_{sq1II}^{\Psi_r} + u_{sq2II}^{\Psi_r} = 2 . (\omega_n . f_{\Psi_r} . i_{sd}^{\Psi_r} - \frac{(1-\sigma)}{\sigma x_H} . n . \Psi_R)$$

**(5-3)**

From the equation (4-3),(5-1),(5-2) it can be said that in the steady state it is possible to regulate the voltage of one inverter to control the $d_1$-and $q_1$ currents and with the other inverter $d_2$-and $q_1$ currents. In the case of transient state the change in the one inverter voltage will cause the currents in the other to change, however the closed loop PI controllers will take care of the imbalance in the $d_1$-$d_2$ and $q_1$-$q_2$ currents.

Thus two sets of the d-q currents are controlled independently of each other by PI regulators to generate the reference voltage vectors $u_{st1}$ and $u_{st2}$ which are displaced in phase by $30^0$.

The modulation technique used in the implementation is the normal Sinusoidal Pulse width with the third harmonic injection which gives nearly same modulation range as that of the space vector modulation.

The flux model used in the realization of the drive is current model as explained in the section 2.4.
The reference current in per unit for the drive is calculated as shown below.

$$i_{sd}^{*\psi_r} = \frac{m_{ref}}{\psi_R} \qquad \textbf{(5-4)}$$

The reference d axis current should be limited to maximum allowed current, as the independent control of the $i_d$ and $i_q$ can only be possible as long as the maximum current in the motor is not reached. The strategy used in the drive for current set points is as described in [B.4] where the $i_d$ is allowed to reach half of the rated per unit current. This allows adequate control margin for the torque producing component $i_q$.

The reference currents are compared with the actual components of the respective d-q currents of the two phases and the error is minimized by the PI regulators. The transfer function of the PI regulators can be expressed as

$$h = K_p \frac{1+T_i.s}{T_i.s}$$

This analog PI controller is discretized by trapezoidal rule to adapt it to the digital signal processing.

The sinusoidal pulse width modulation technique is used to generate the command signals to the switches. Two modulators are used with the same triangular carrier signal and six modulating signals as shown below.

$$u_{sta1}(t) = u_{st1}\left[\cos(\zeta_1(t)) - \frac{1}{6}.\cos(3.\zeta_1(t))\right]$$

$$u_{stb1}(t) = u_{st1}\left[\cos(\zeta_1(t) - 120^0) - \frac{1}{6}.\cos(3.\zeta_1(t))\right]$$

$$u_{stc1}(t) = u_{st1}\left[\cos(\zeta_1(t) - 240^0) - \frac{1}{6}.\cos(3.\zeta_1(t))\right]$$

$$u_{sta2}(t) = u_{st2}\left[\cos(\zeta_2(t) - 30^0) - \frac{1}{6}.\cos(3.(\zeta_1(t) - 30^0))\right]$$

$$u_{stb2}(t) = u_{st2}\left[\cos(\zeta_2(t) - 150^0) - \frac{1}{6}.\cos(3.(\zeta_1(t) - 30^0))\right]$$

$$u_{stc2}(t) = u_{st2}\left[\cos(\zeta_2(t) - 270^0) - \frac{1}{6}.\cos((3.\zeta_1(t) - 30^0))\right]$$

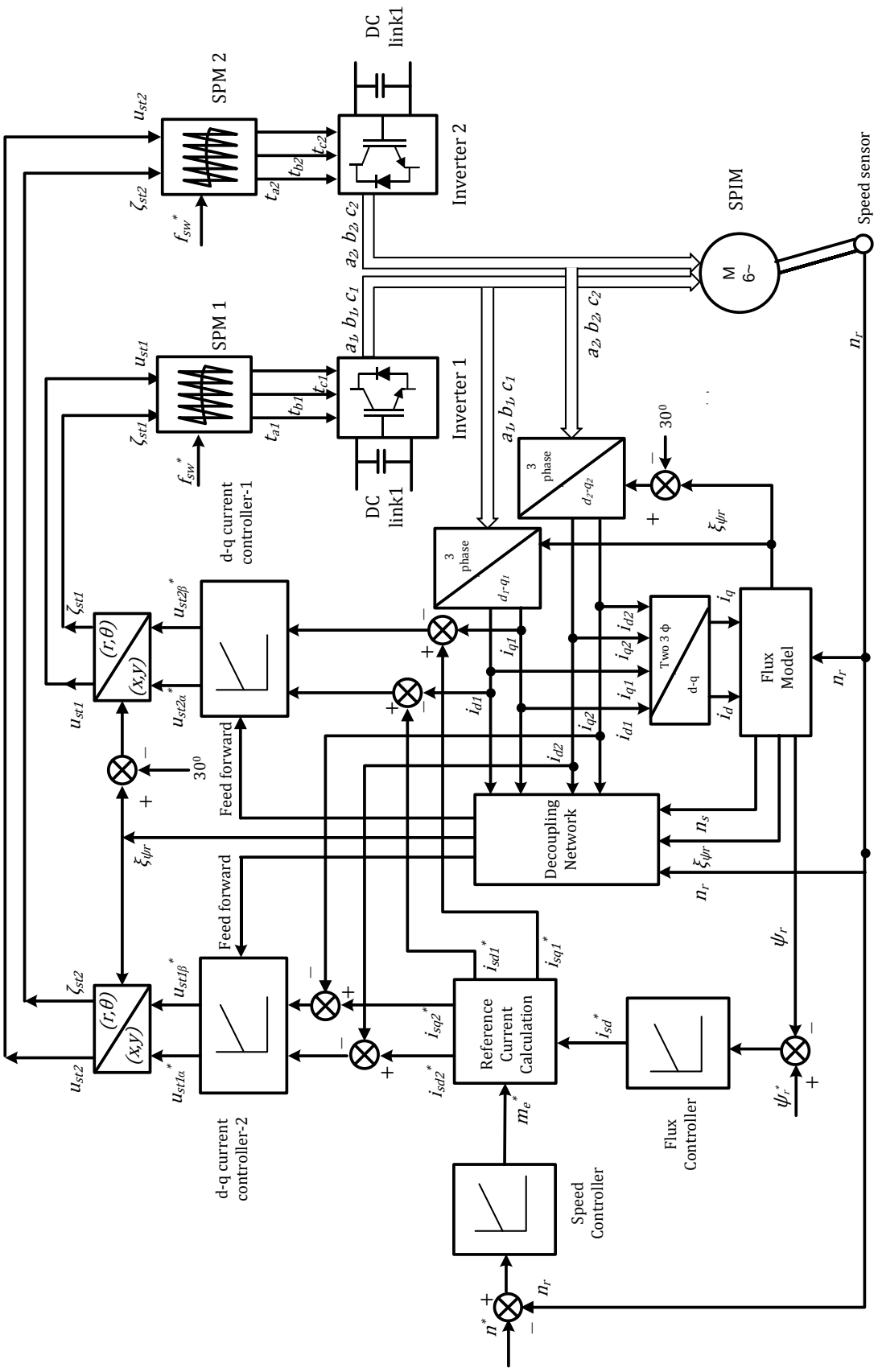


**Figure 5-1: Block diagram of Double Synchronous frame Current Control.**

## 5.2. Decoupled Current Control.

The decoupled current control strategy as proposed in [12] for the PMSM is also implemented and evaluated in the thesis.

In the decoupled control the two sets of PI regulators are used for controlling the d-q and the z subspace currents.

The relations ship that is mentioned in equation (4-3) can be written for the currents as shown below

$$\begin{bmatrix} i_d^s \\ i_q^s \end{bmatrix} = \frac{1}{2}\left\{\begin{bmatrix} i_{d1}^s \\ i_{q1}^s \end{bmatrix} + \begin{bmatrix} i_{d2}^s \\ i_{q2}^s \end{bmatrix}\right\} \tag{5-5}$$

And for the z subspace currents

$$\begin{bmatrix} i_{z1}^s \\ i_{z2}^s \end{bmatrix} = \frac{1}{2}\left\{\begin{bmatrix} i_{d1}^s \\ -i_{q1}^s \end{bmatrix} + \begin{bmatrix} -i_{d2}^s \\ i_{q2}^s \end{bmatrix}\right\} \tag{5-6}$$

The inverse relationship back in terms of individual d and q currents can be written as

$$\begin{bmatrix} i_{d1}^s \\ i_{q1}^s \end{bmatrix} = \left\{\begin{bmatrix} i_d^s \\ i_q^s \end{bmatrix} + \begin{bmatrix} i_{z1}^s \\ i_{z2}^s \end{bmatrix}\right\}$$

$$\begin{bmatrix} i_{d2}^s \\ i_{q2}^s \end{bmatrix} = \left\{\begin{bmatrix} i_d^s \\ i_q^s \end{bmatrix} + \begin{bmatrix} -i_{z1}^s \\ i_{z2}^s \end{bmatrix}\right\} \tag{5-7}$$

These relationships are very important as it allows the control of the d-q currents by controlling the z axis currents in the close loop.

The stator voltage equation can be written in the time delay element format in terms of the individual d-q currents as shown below.

$$\frac{d(i_{sd1}^{\Psi_r}+i_{sd2}^{\Psi_r})}{dt} = -\frac{1}{T_s''}\left(i_{sd1}^{\Psi_r} + i_{sd2}^{\Psi_r}\right) + \omega_n . f_{\Psi_r} . (i_{sq1}^{\Psi_r} + i_{sq2}^{\Psi_r}) - \frac{(1-\sigma)}{\sigma T_r} . \frac{\Psi_R}{x_H} + \frac{\omega_n}{x_\sigma} . 2 . u_{sd}^{\Psi_r}$$

$$\frac{d(i_{sq1}^{\Psi_r}+i_{sq2}^{\Psi_r})}{dt} = -\frac{1}{T_s''}(i_{sq1}^{\Psi_r} + i_{sq2}^{\Psi_r}) - \omega_n . f_{\Psi_r} . (i_{sd1}^{\Psi_r} + i_{sd2}^{\Psi_r}) - \frac{(1-\sigma)}{\sigma x_H} . n . \Psi_R + \frac{\omega_n}{x_\sigma} . 2 . u_{sq}^{\Psi_r} \tag{5-8}$$

Similarly

$$\frac{d(i_{sd1}^{\Psi_r}-i_{sd2}^{\Psi_r})}{dt} = -\frac{1}{T_s''}\left(i_{sd1}^{\Psi_r} - i_{sd2}^{\Psi_r}\right) + \frac{\omega_n}{x_\sigma}.2.u_{sd}^{\Psi_r}$$

$$\frac{d(-i_{sq1}^{\Psi_r}+i_{sq2}^{\Psi_r})}{dt} = -\frac{1}{T_s''}\left(-i_{sq1}^{\Psi_r} + i_{sq2}^{\Psi_r}\right)+.2.u_{sq}^{\Psi_r}$$

**(5-9)**

The detail schematic of the control strategy is shown in the Figure 5-2.
In the control scheme the same flux model is used, however to implement the control strategy the six phase transforms are employed which converts the two groups of three phase currents directly to the six phase d-q in the rotor reference frame.
The structure of the software code employed to test this control scheme is same as that of the earlier control scheme. The only change is done while the calculating the current references, while calculating the current references the transforms have to use for the individual subspace.
As seen from the equation (5-9) for the z1-z2 subspaces, it can be seen that the z controllers try to balance out any imbalances occurring between the two three phase groups by controlling the z currents induced in the stator winding. However up to what extent the z axes controllers manage to balance out these imbalances need to be investigated.

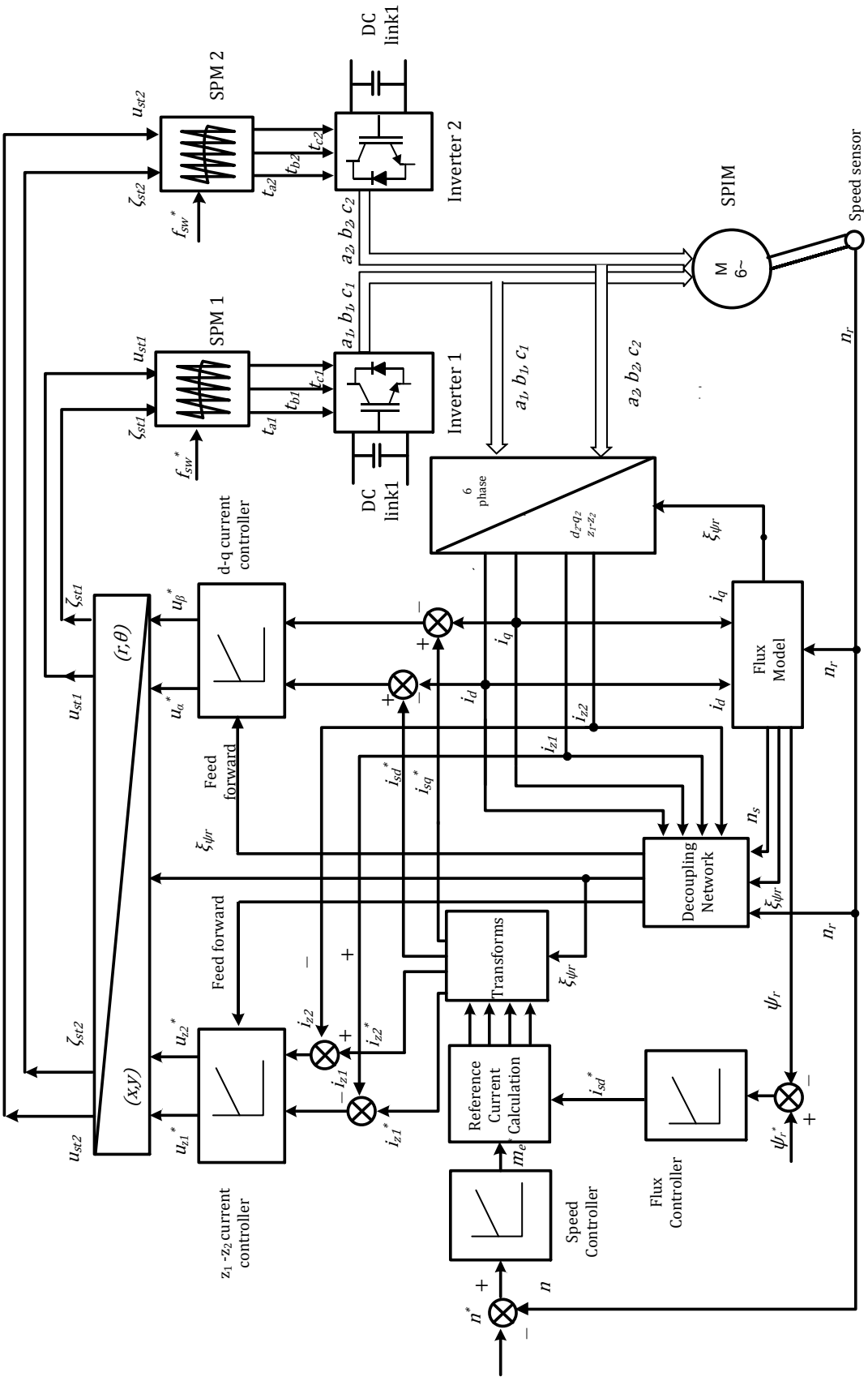


**Figure 5-2: Block diagram of the Decoupled Control Strategy.**

# 6. System Synoptic and drive Implementation.

Building of the drive has to be carried out on the two stages hardware implementation and software organization with debugging activity alongside. In the following section the system overview of the drive system under test as well as the software structure and the development is discussed.

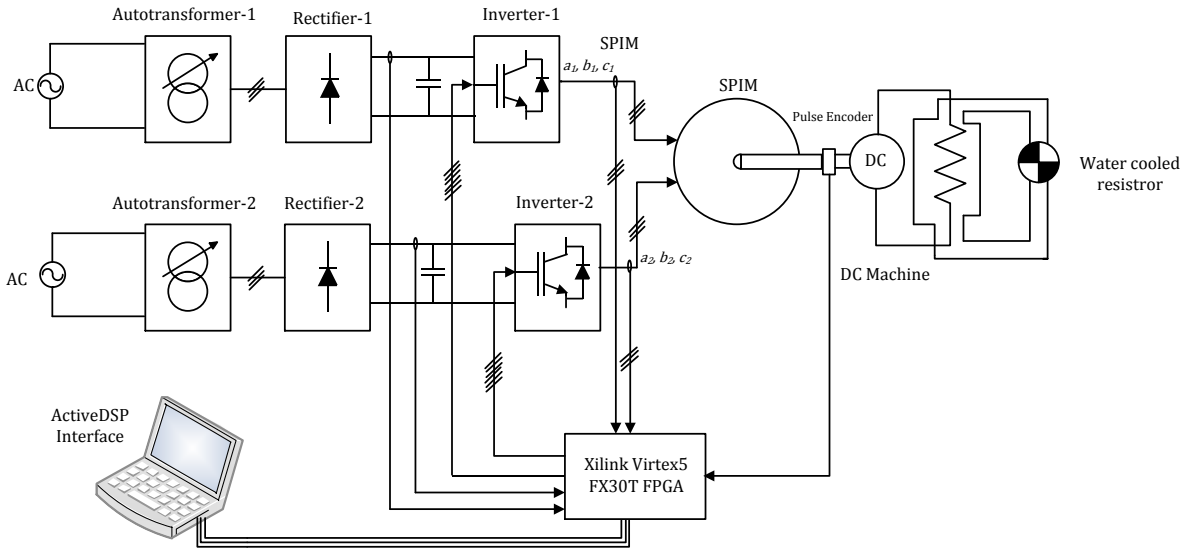


**Figure 6-1: System Synoptic of the test rig.**

Above figure shows the synoptic of the test rig that is used for the actual implementation and evaluation of the performance of the SPIM

As shown in the figure two three phase inverters fed with separate rectifiers are used to drive the SPIM. Pulse encoder is used to get the rotor position.

The two inverter modules are controlled using the FPGA control card. The control card is programmed by using the eclipse based platform viz. Xilink SDK (Software Development kit) available in the Xilink ISE development suit 12.3.The necessary IP modules on FPGA are provided by SINTEF for drive control.

The control card is connected to the have the PC interface via Active DSP version 1.507 for online monitoring of the various parameters.

The induction machine is loaded using the DC generator.

## 6.1. Software Implementation.

In the following section the structure of the software for the drive is discussed. The program skeleton is based on the structure that is used for a three-phase grid-connected active rectifier in the SINTEF Energy Lab [19].
The drive profile is based on the Drivecom standard [22]. The state machine is used in the software is provided by Roy Nilsen of Wartsila.

### *6.1.1 Program Structure.*

The program structure is summarised in the Figure 6-2 .

The standard C start-up routine main() is located in a framework file, ramme.cpp. The start routine contains the initialize files which initializes all the drive parameters as well as configures various FPGA modules.

The background routine is empty; it does not contain anything. The program is having two interrupts one is fast and other is slow. Fast interrupt contains inner current control loop whereas in the slow interrupt the speed and flux control is carried out.

The fast interrupt occurs at the interval of 0.3 ms. Following tasks are carried out in the fast interrupt routine

**a.** A/D conversion of the stator currents.
**b.** Overcurrent and DC link Protection.
**c.** Co-ordinate transformations.
**d.** Updating of flux model.
**e.** Current control.
**f.** Conversion of d-q currents to stator coordinates.
**g.** Updating the reference to PWM Modulator.

The slow interrupt is having period of 1.5 ms which contains following tasks

a. Flux control.
b. Speed control.

The entire program for the drive is attached in the appendix.

### *6.1.2 The State Machine*

This is the subroutine which controls the logical switching conditions of the program. There are mainly eight states defined as below.

**a.** Not ready to switch on.
**b.** Switch on disabled.
**c.** Ready to switch on.
**h.** Switched on.
**e.** Operation enabled.
**f.** Quick stop active.
**g.** Malfunction.
**h.** Identification.

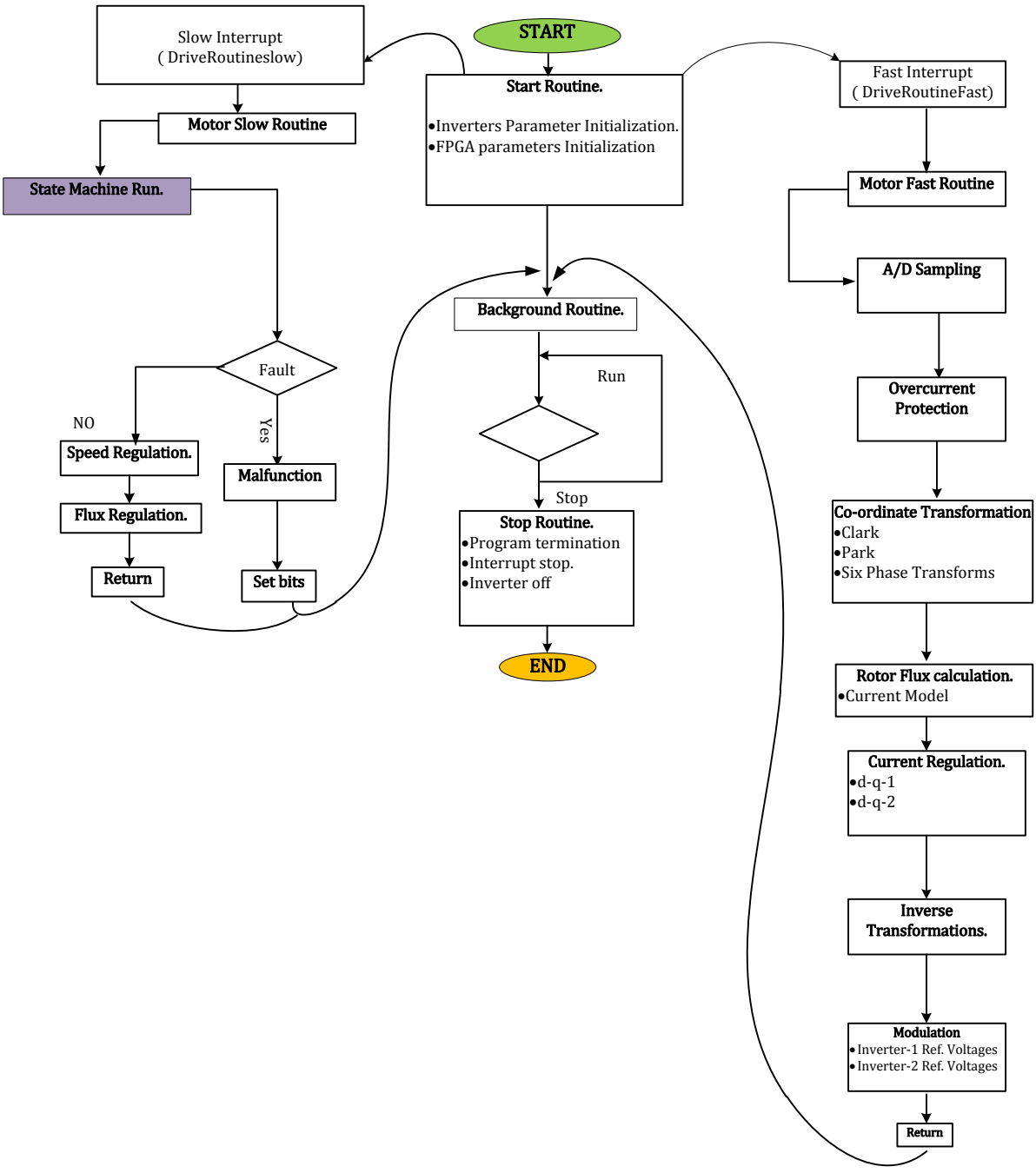


**Figure 6-2: The Program structure.**

The state machine haves following important words to carry the information to and from the state machine.

i. **Motor Control Word.**
This is the main control word. By setting or resetting various bits in the word the internal events of the state machine or the sequence can be changed.

ii. **Motor Status Word.**
The current status of the drive state machine is read by the status word.

iii. **Motor Fault Word.**
This word holds the information about various faults occurring in the motor as well as inverter.

iv. **Motor Warning Word.**
This word indicates that particular limiting parameter of the inverter and the motor is reached or not.

### *6.1.3 Motor States.*

The state machine switches to different states depending on the different operating conditions that prevail in the Induction machine as well as in the inverters. In the subsequent paragraph the description for the state machine is described.
The machine is in 'Not Ready to Switch On' prior to power on. After powering on control and drivers circuits it goes to 'Switch on Disable' state.
The state is changed from the 'Switch on Disable' to 'Ready to Switch on' when both the DC links are charged, and the command from the user to enable the voltage is received. In 'Ready to Switch on' state the pulses to the inverters switches are still blocked and user is allowed to made selection for the identification run. On selection of the identification run the machine switches to 'Identification run'. The 'Identification run' state is retained till the parameter identification is not completed. When the identification run is completed the machine switches back to the 'Ready to Switch on' state. The machine then switches to the 'Switched on' state; in this state the pulses for the inverters are released and magnetization is carried out. When the magnetization is finished the machine switches to 'Operation Enable' and the drive is started.
In each state the malfunction word is checked, if some fault occurs in any state the respective bits in malfunction word is set, and machine goes to the 'Malfunction' state.
The conditions to shift the various states and the various states are as shown in the Figure 6-3.

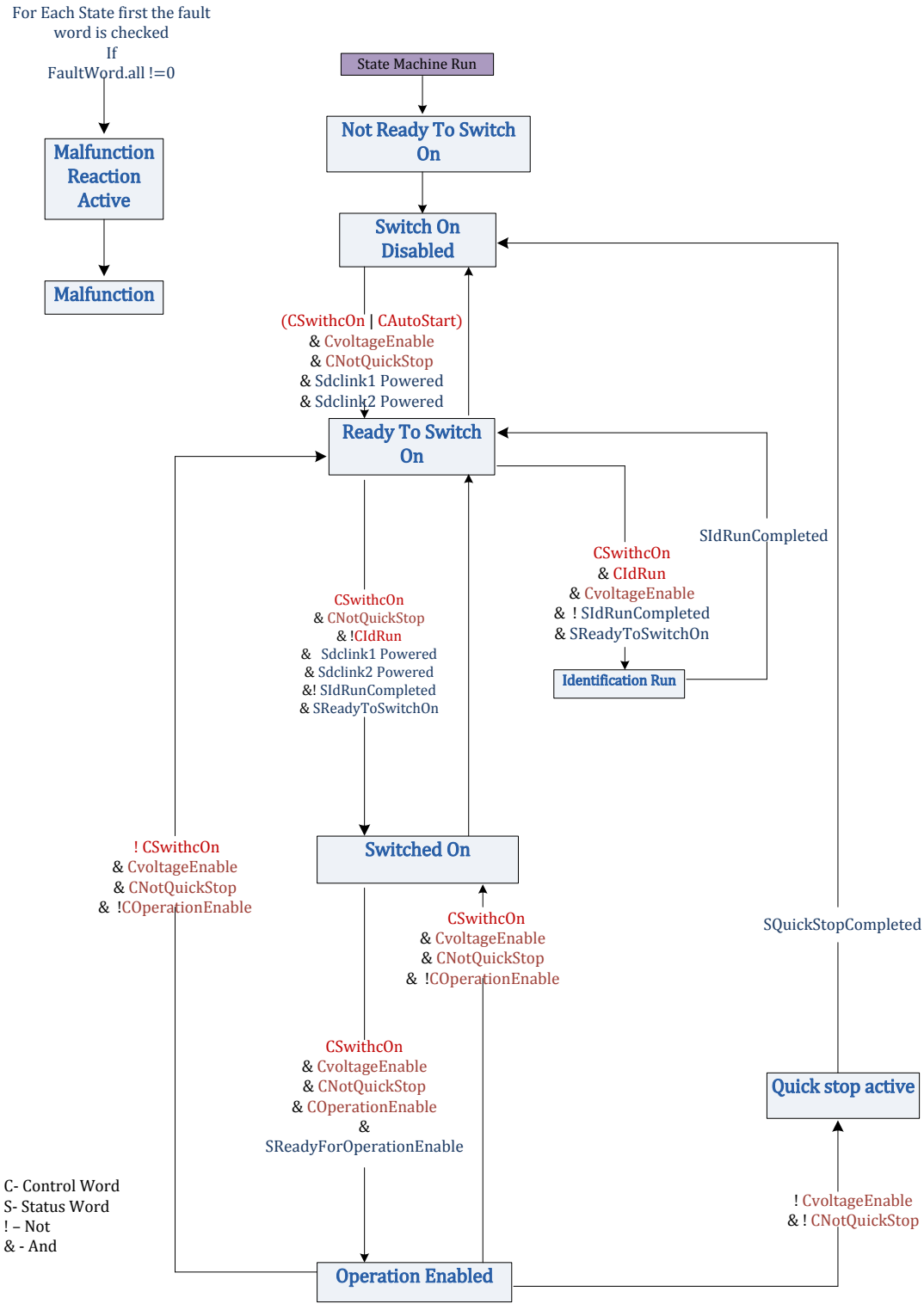


**Figure 6-3 : The State Machine**

## 6.2. Hardware Implementation.

Following section describes the hardware components that are used in the implementation of the drive.

### *6.2.1 FPGA Control card.*

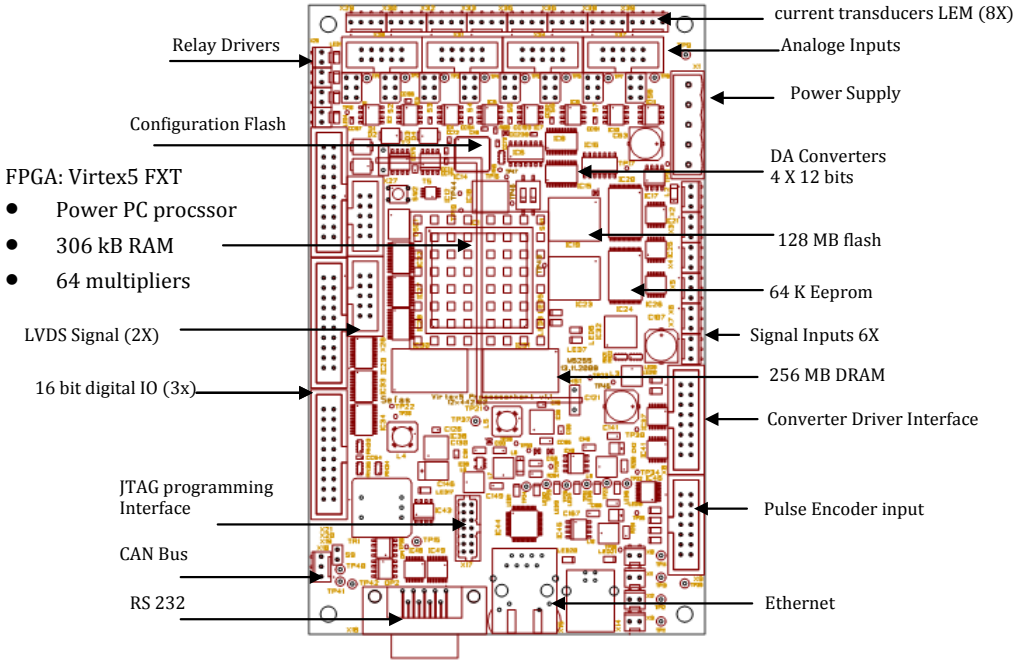


**Figure 6-4: FPGA Control card [17].**

For the control purpose the Xilinx Virtex5-XC5V FX30T FPGA chip is used, the control card outline with the chip and other important peripherals is as shown in the Figure 6-4. The control card is specially developed by SINTEF to suit the various requirements for different power electronic control applications. The important components of the control cards apart from FPGA are mentioned below.[16]

**a. Communication ports:**

The card is having RS232 serial port connected with a male 9 pole D-sub connector. The serial port is not isolated. Ethernet port for 10MB/sec and 100 MB/sec connection is available on board. The port is based on the MAC block which is embedded in the Virtex 5 chip. The standard physical interface (PHY) is located on the separate chip (National Semiconductor DP83848) outside FPGA on the board. The board is also having the high speed V.2 USB port with the separate controller NXP ISP1582 available on board outside FPGA.

CAN controller IC, Microchip MCP2515, is available on card for the with the other control cards

**b. Memory:**

Card is having ample amount of memory as summarized below.

- DDR2 DRAM - Micron MT74H64M16HR-3E in 1GB, 16x64Mbit 333MHz clock frequency.
- EROM- Renesas HN58V257A. 32k x 8 bits.
- FLASH- Spansion S29GL512P is 512 Mbit flash chip, 32Mx16 64Mx8.

**c. Clock:**

The FPGA is supplied with the 40 MHz clock on the card. FPGA generates different clock frequencies inside which are used by various components are as listed below.

- AD-converter is operated with a differential 40 MHz clock.
- AD converter generates a 240 MHz clock. This drives the transfer of data from the AD converter.
- USB controller is powered with a 12 MHz clock.
- CAN controller is driven by a clock of 20 MHZ.
- Ethernet PHY circuit is run a 25 MHZ clock.
- The RISC processor is powered by a 300 MHz (PowerPC) or 100 MHz (Micro Blaze) clock.
- Processor bus powered by a 100 MHz clock.
- DDR2 DRAM chips driven by a differential clock of 200 MHz.
- Transport correction (IDELAYCTRL) for DDR2 DRAM is run by a 200MHz clock.

**d. Inverter Driver Interface.**

The card has the separate output port for the signals to the inverters as shown in the Figure 6-4. Signal level is 4 V CMOS and the control signals are active high. Two power switches in a bridge-leg are controlled by two separate signals and a common on signal for all transistors. Feedback signal from the inverter is common OK signal which is active high and four bit status signal (0000) which is active low .This code is defined as inverter error /reset / voltage / offline. The code can be found in the appendix.

**e. Pulse Encoder.**

Card has input for connecting a two-phase encoder with a reference signal. The signals are adapted to a Heidenhain ROD 420 pulse encoder, which has balanced signals with RS422 signal levels. Pin numbering is the same pin numbers on the Round 12 pole connector ROD420. Receiver circuit MAX3097 detects signal on lines. Three green LEDs at the connector can be used to indicate the signal levels from the pulse sensor, while a red LED can be used to indicate errors.

f. **Relay drivers.**

Card is equipped with four relay driver. The output voltage is 5V.This is sufficient to run many types of relays with coil voltages 6V. Small cooling fans can be operated with this. An LED illuminates when a relay driver is turned on.

**g. LVDS.**

The card is having contacts for high speed serial communication with LVDS signals having 600 Mbit/sec. transfer rate. LVDS transmission line has 100 Ω differential line impedance. The line pair is terminated on FPGA with 100 Ω resistance between lines.

**h. Signal Inputs**

The card is having six general purpose signal inputs either analog or digital .The analog signals are read through the voltage divider network and with low pass filter with 30 µ sec time constant signal level for the analog signal is 0-5 V. Digital signals are inputted through the low pass filter with 1 µ sec time constant, the signal level being 5 V CMOS.

i. **AD Converter**

The card is equipped with an Analog Devices AD9222, 8-channel 12-bit AD converter. Each channel has its own AD converter that works with 40 MSPS. The channels thus sampled synchronously. Data is transferred to the FPGA in a serial form, the baud rate is 12BIT x 40 MSPS = 480 Mbit/ sec rates.

**j. Digital Input Output port.**

There are three channels on card with 16 bit digital IO ports. The signal level is the 0-3V. This can drive 5V TTL inputs; however as the FPGA block is fed with the 3 volts so voltage is clipped before entering into FPGA.

### *6.2.2 FPGA IP Modules .*

On the FPGA various IP modules can be made out of the logic gates and input outputs to perform the specific tasks. In the drive following IP modules are used which are provided by SINTEF .

- AD converter serial signal interface
- Pulse Encoder Interface.
- Inverter Interface.
- Accumulator filter block.
- Pulse Width Modulator.
- Comparator Limiter.

These modules are hooked up to the processor local bus so that these can work along with the processor available on the FPGA chip. The code for the configuration files for the various IP modules can be found in the appendix.

### *6.2.3 Control board.*

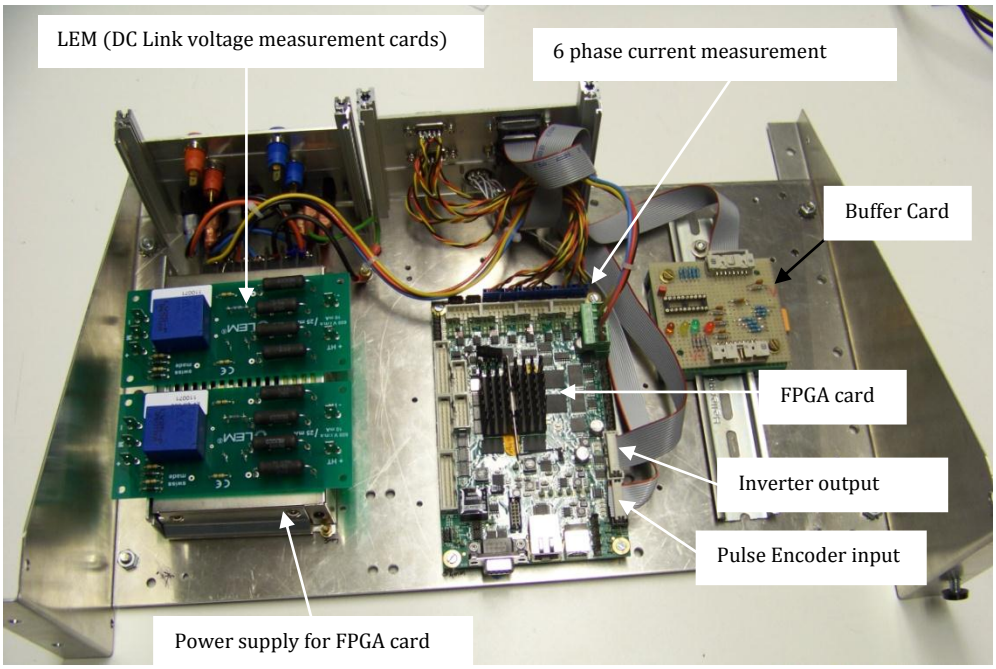


**Figure 6-5: Control Board.**

Above figure Shows the control board. This is the command and control of the drive; this includes low voltage control components.

The Control board includes
a. The LEM sensors for DC link voltage measurement.
b. The Pulse Encoder measurement connections.
c. Signal and power connections to the LEM current sensors.
d. Power supply for the control card.

### *6.2.4 Currents and voltages measurements.*

Line current measurements are performed by LEM transducers, LA205-S type based on Hall Effect sensor. The LEMs are directly mounted on the inverters to sense the line currents. LEMs are powered by the +15 volts supply on the card. The A/D converter on the card samples the six line currents at the frequency of 40 MHz; the sampled currents are then down-sampled to 0.1 MHz with the help of the filter on the FPGA card. The down sampled currents are further filtered with the help of the moving average filter in the FPGA to avoid the unwanted ripple that occurs at the sampling time. This sampling signal for one electrical period is shown in the figure Figure 6-6 . The readings in the pink are the discrete current readings from the A/D converter; the red points are the average values, while the yellow are the filtered values. It can be seen that the filtered waveforms are smooth. The advantage of sampling and integrating the values at these high rates ensures that the transient currents between the two PWM sampling periods will get captured by the software and the over current protection will come into action to trip the system.

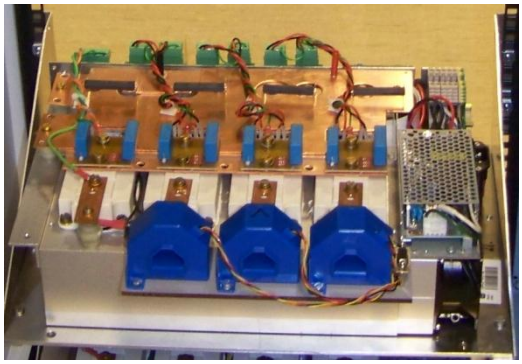

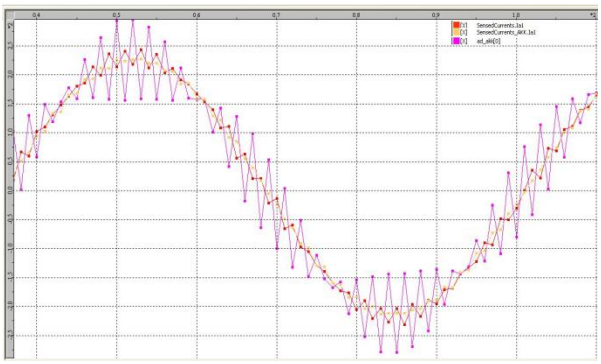

**Figure 6-6: LEM Current Transducers and sensed currents**

The two DC link voltages are sensed by the LEM sensors (LV 25-600) cards that are mounted on the Control board as shown in the
Figure 6-5: Control Board.. The same method is used as that of currents for the DC links voltages measurements, however the moving average filter is not used in this case since DC link voltage remains constant most of the time.

### *6.2.5 Rotor Position Measurement.*

In the vector control it is required to have the instantaneous rotor position for estimation of rotor flux vector position as well as the current transformations. Various analog and digital methods exists to find out the rotor position such as potentiometers, synchros, resolvers, absolute and incremental encoders. In the implementation of the six phase motor drive the incremental encoder of Heidenhain make (model- ROD 420) is used. Refer appendix for the data sheet.

### *6.2.6 Inverter Modules.*

These are main power processing unit of the drive, air cooled inverter modules designed by SINTEF for the laboratory purpose at NTNU are used. Having following salient features.

**Overload protection-** The temperature of the cooling fins are measured for overload protection, at high temperature the drivers will block any signal to the inverters.
**Over current and SC protection-** The driver cards monitor the voltage $v_{ce}$ when the voltage drop across collector and emitter becomes high due to over-current or SC the drivers block the signals to inverters.
**High DC link protection-** The chopper control card monitors the DC link voltage, if the voltage goes high the card switch on the IGBT to discharge the DC link capacitor to the external braking resistor.
The inverter has a Hex display board which the status of the inverter is displayed

Detail technical specifications of the inverter can be found in Appendix

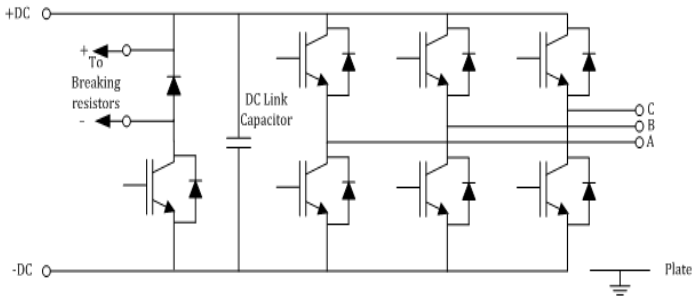


**(a). Circuit Diagram**

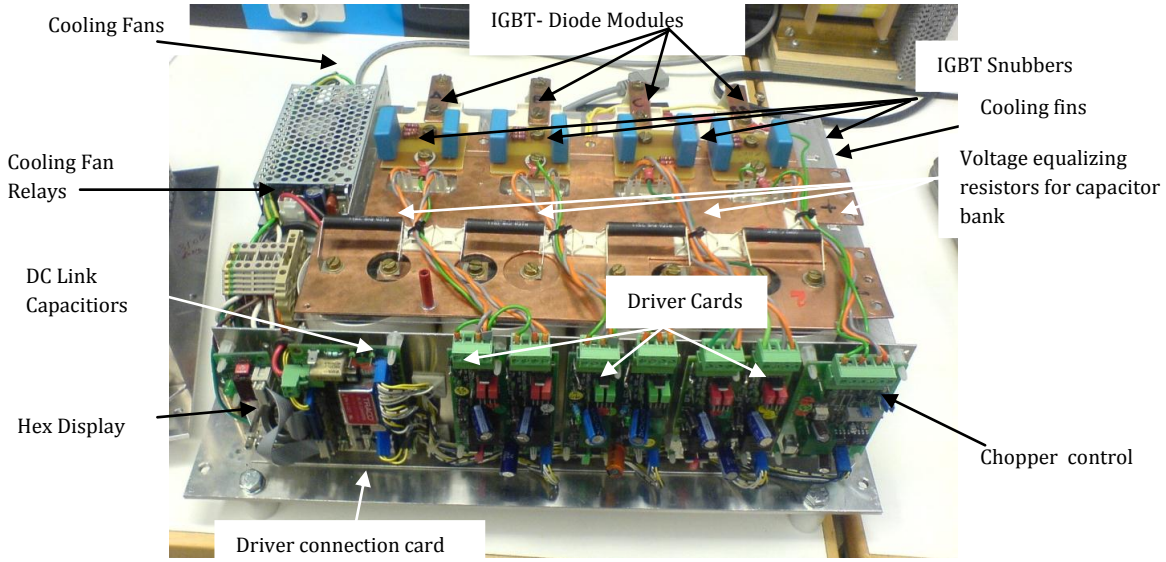


**(b). Inverter Module.**
**Figure 6-7. Three phase IGBT Inverter.**

### *6.2.7 Converter.*


**Figure 6-8. DC Rectifier**

The inverters are fed through the rectifiers these are standard modules available at the university as shown in the figure above. Rating of the converter is as below.

- Voltage input (rms) – 0-400 V AC.
- Voltage output – 0-600 V DC.
- Current – 63 Amps.

### *6.2.8 Six Phase Induction Motor.*

The six phase machine specially made for the evaluation for the control has following specifications

- Power output – 11.7 kW
- Voltage (Line to line rms)- 400 V star connection
- Current ( line rms) – 11.8 Amps.
- Rated Speed – 2235 rpm
- Maximum speed – 5000 rpm
- Rated frequency – 75 Hz
- Rated Torque – 50 Nm
- Power factor – 0.77

### *6.2.9 Assembly of the drive.*

Following picture shows the snapshot of the drive test set up.The transformer is used to provide the galvanic isolation to the drive power supply form the AC grid. The converters are supplied by three phase auto transformer.

The auto transformer that supplies the two converter DC link can charge DC link up to 325 Volts so the motor cannot be operated with the rated conditions since the inverters goes to saturation before the rated conditions are reached. This limitation has to be overcome to test the drive up to its rated condition.

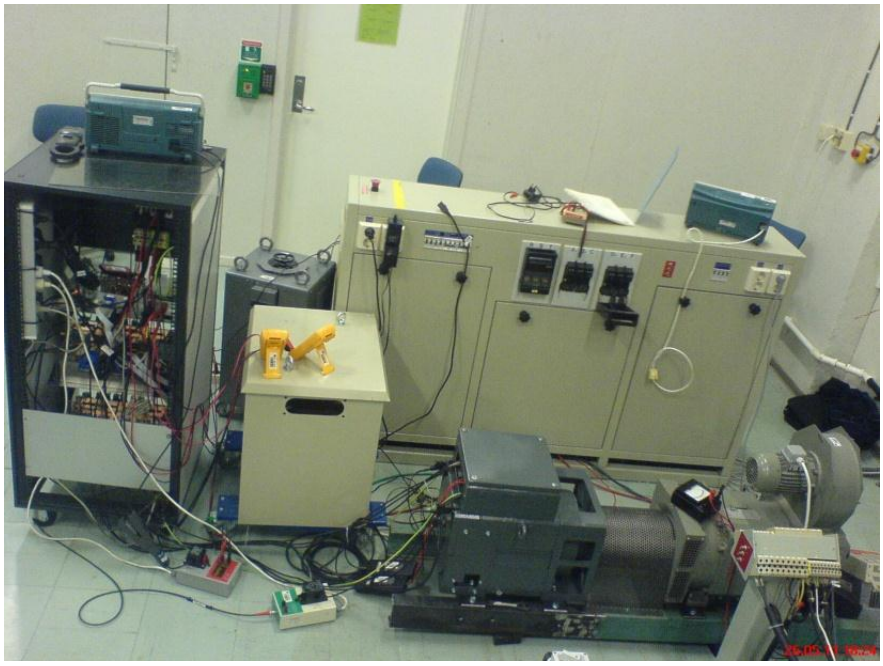

**Figure 6-9: The test drive set up**

# 7. Comparison of Simulations and Actual Results on the drive.

## 7.1. Introduction.

The DSFCC control strategy is tested for the following test cases and the simulations are compared with the actual result obtained on the Six Phase Induction Motor.

1. Normal operation with same DC link Voltage in both the inverters and same torque references.
2. Normal Start up with the same DC link Voltages and then torque reduction in the one of the inverter
3. Trip of one inverter
4. Operation with different DC link voltage.

In the following sub section the DSFCC control strategy is discussed.

### 7.1.1 *Normal operation with the step change in the torque reference for the both inervters.*

The simulation results are shown in the Figure 7-1. It can be seen from the simulations that the magnitude of the z currents induced during the steady state operation is negligible.
The total line currents in case of the 0.4 pu torque reference and 0.5 pu direct axis current is around 0.6 per unit currents

Figure 7-2 shows the actual results on the drive with the $i_d$ keeping 0.5 pu and the 0.4 pu ramp increase in the iq reference of the both inverters. The result is real time plot in the Active DSP. The regulator response can be seen from the figure. The ramp is used to avoid sudden transient in the system. It can be seen that under balanced condition the $z_1$-$z_2$ currents are almost zero.

Figure 7-3 shows the oscilloscope traces of the actual currents in the both the phase group, it can be seen that it is about 0.6 pu which is equal to the resultant of the d and q axis currents.

While taking the readings of the motor currents the 2.9 kHz filter on the oscilloscope is turned on to filter the spikes due to blanking time of the IGBTs.

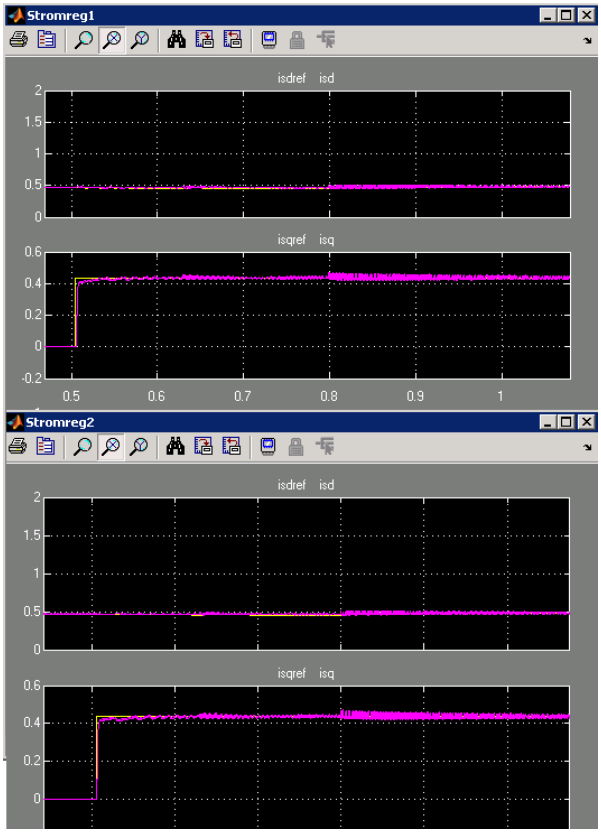


a. d-q Currents

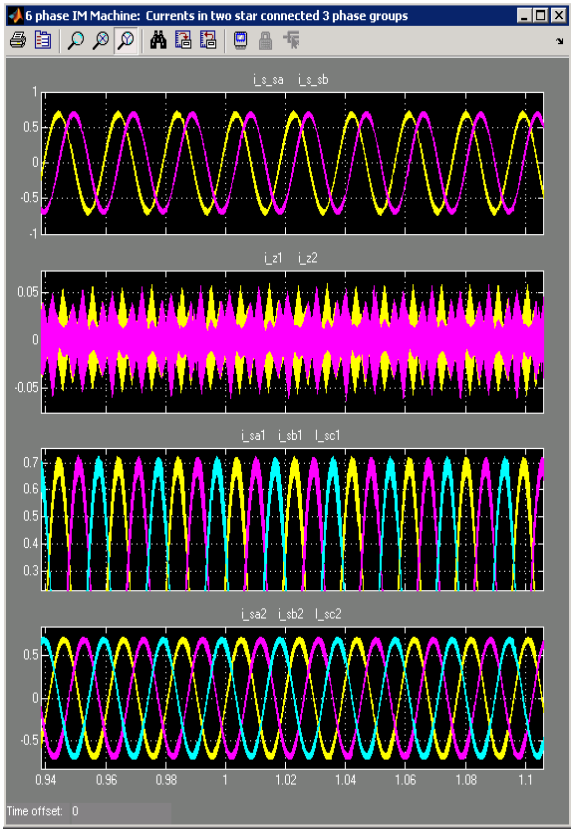


b. Line Currents

**Figure 7-1 : Simulation results for the step change in the torque reference.**

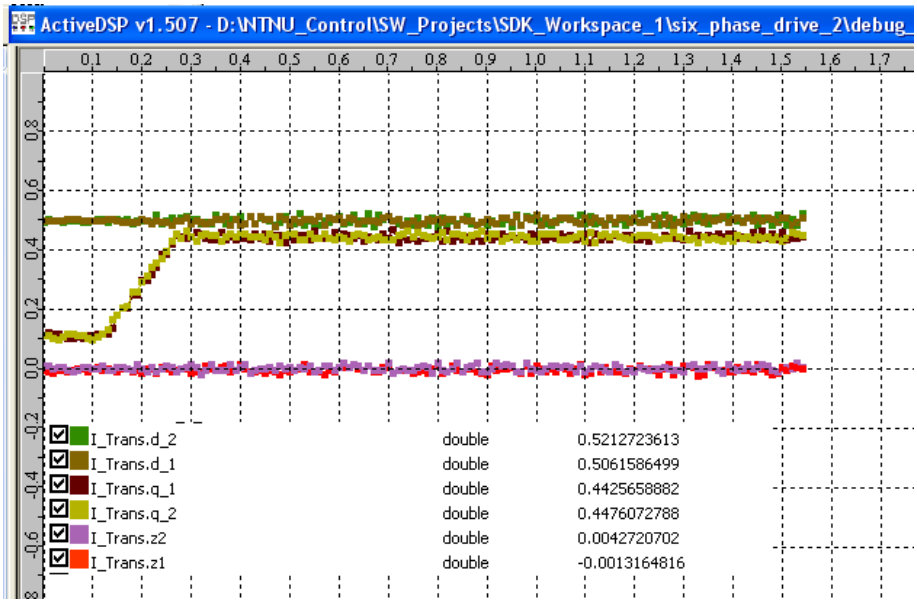


**Figure 7-2 : Ramp input in the $i_q$ Real time DSP trace**

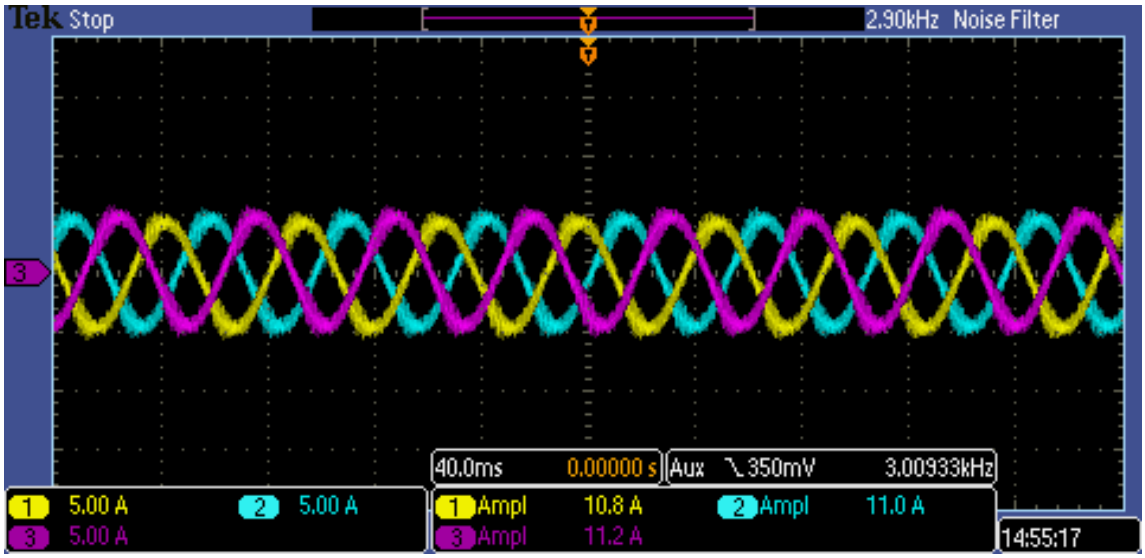


**a. Currents in the Phase Group 1**

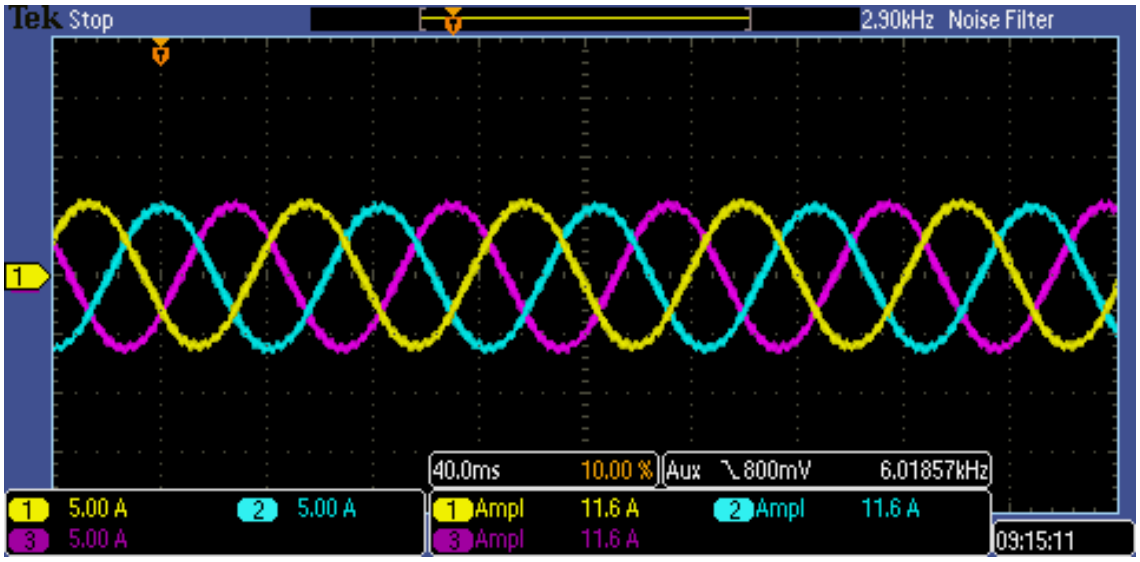


**b. Currents in the Phase Group 2**

**Figure 7-3 : Oscillogram traces of the Actual Motor Currents**

### *7.1.2 Normal operation with the same DC link voltages and the reduction in the torque reference of one of the inverter.*

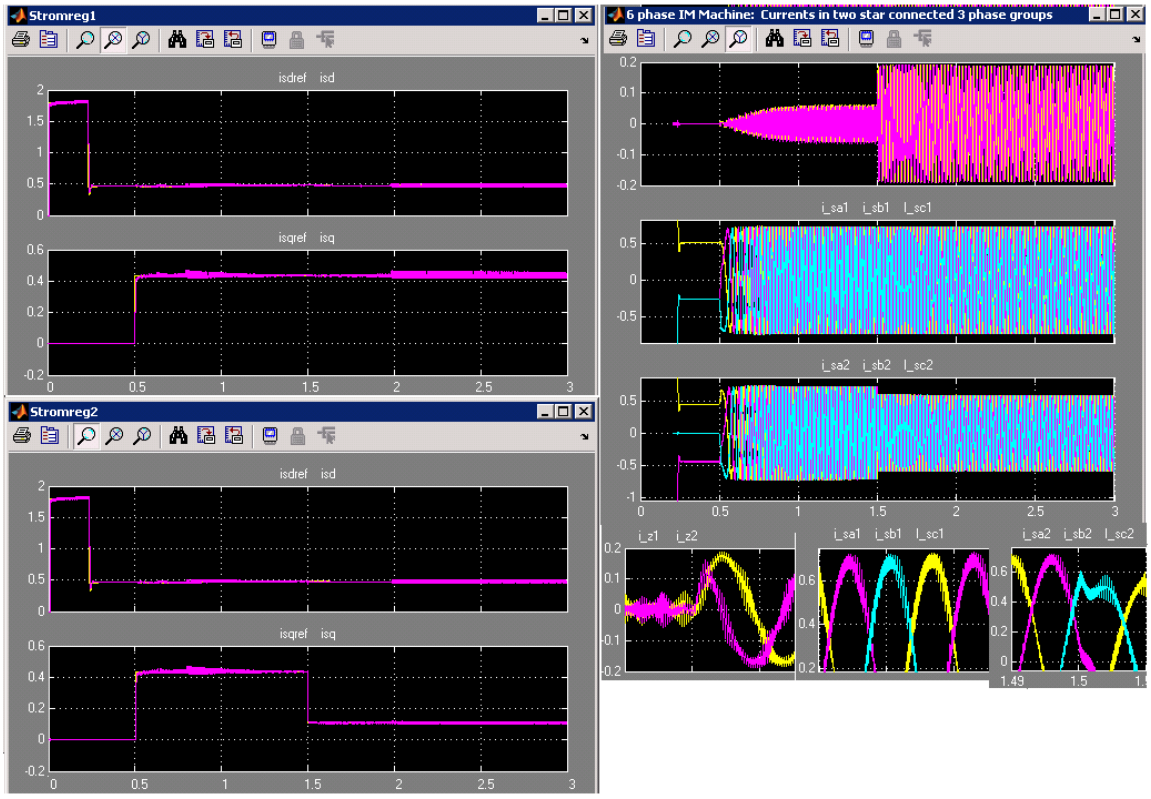


**Figure 7-4: Simulation results of the step reduction in the inverter 2 for DSFCC**

Figure 7-4 shows the simulation results, the torque reference of the inverter 2 is reduced from the 0.4 pu to 0.1 pu It can be seen that the z components are getting induced as the result of this the magnitude of the z axes currents can be seen as 0.2 pu peak.

The current in the inverter 2 is reduced as the result of the reduced torque Bridge leg module reference; the magnitude can be seen as 0.56 pu from the simulations.

The actual results are as shown in the Figure 7-5 , torque reference of the inverter 1 is reduced from the 0.4 to 0.1 as it can be seen in the figure the z components are getting induced, however when the torque reference is again increased the motor reaches its previous operating state. It was also observed that the motor speed is reduced when the torque reference is reduced.

From the Figure 7-6 it can be seen that the pu currents flowing in the phase group a is around 0.5 pu, which is in agreement with the simulation.

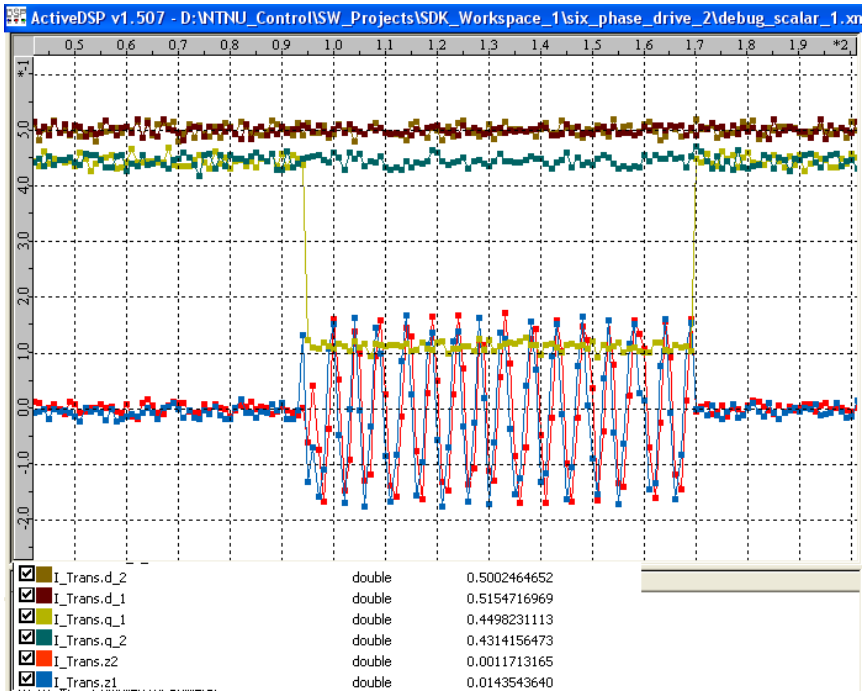


**Figure 7-5 : DSP trace of machine currents**

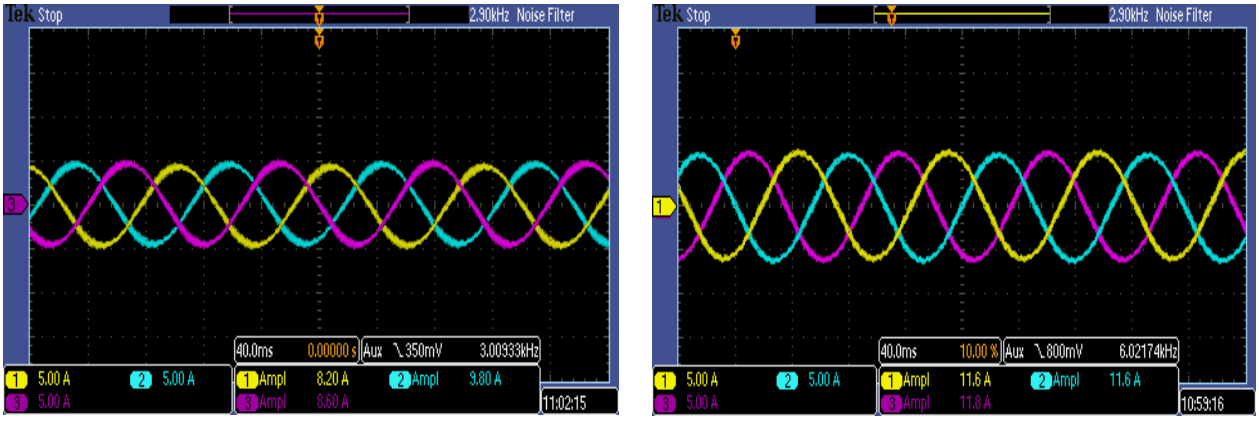


a. Phase Group 1 b. Phase Group 2

**Figure 7-6: Oscillogram traces of the Actual Motor Currents**

### *7.1.3 Trip of one of the inverter.*

In this case one of the inverter is tripped to evaluate the performance of the drive. From the Figure 7-7 it can be seen that the when the inverter 2 is tripped the inverter 1 has to supply all the torque producing current. The line currents of inverter 1 are increased after the fault. This simulation is carried out at the load below the rated so that the inverter one has proper margin in currents to supply the load. The z system currents are induced as the result of the trip of inverter 2, the magnitude of the currents can be seen as 0.5 pu.

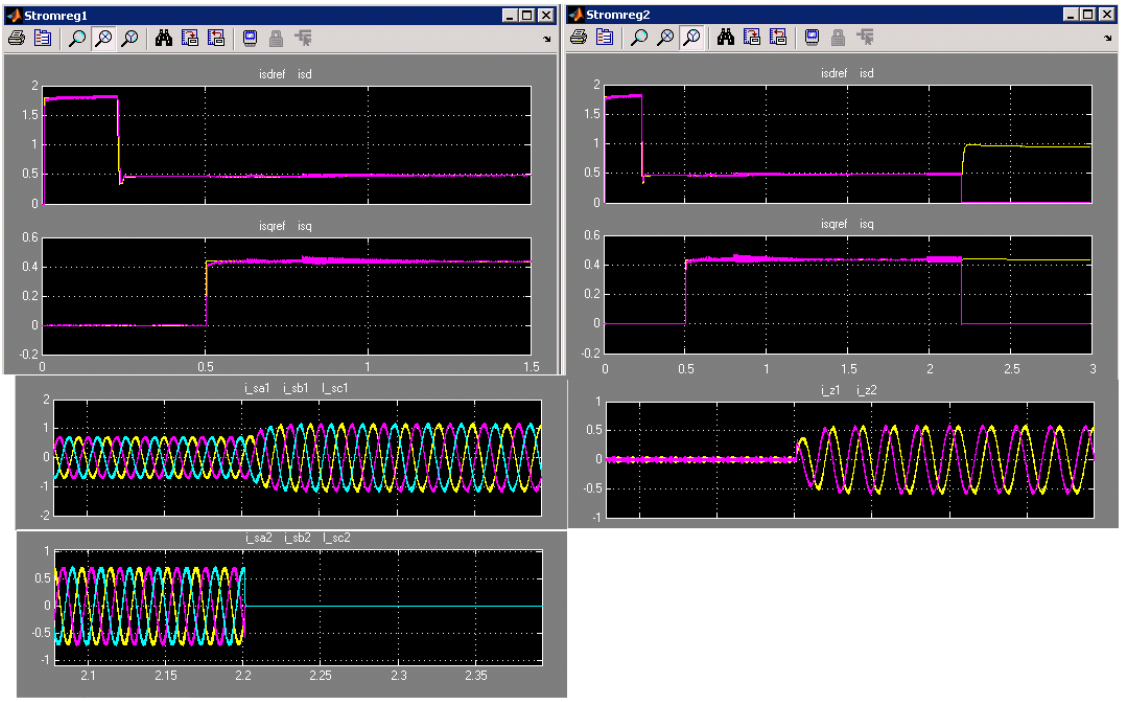


**Figure 7-7: Trip of inverter 2.**

The trip case is also actually tested on the motor drive by disabling the pulses to the inverter 1, the results are shown in the Figure 7-8, both the d and q axis components supplied by the inverter 1 goes to zero as the result of the trip, the amount of z axis currents induced as seen from the figure is 0.4 pu which is nearly matches the simulation results.

It was observed that drive continues to run even if one inverter is tripped if the other inverter has sufficient margin to supply the motor. However if the motor is loaded fully healthy inverter also trips due to large over-currents

There is the mismatch between actual and simulated the currents in inverter of the healthy phase group due to the loading is not exactly simulated in the simulation.

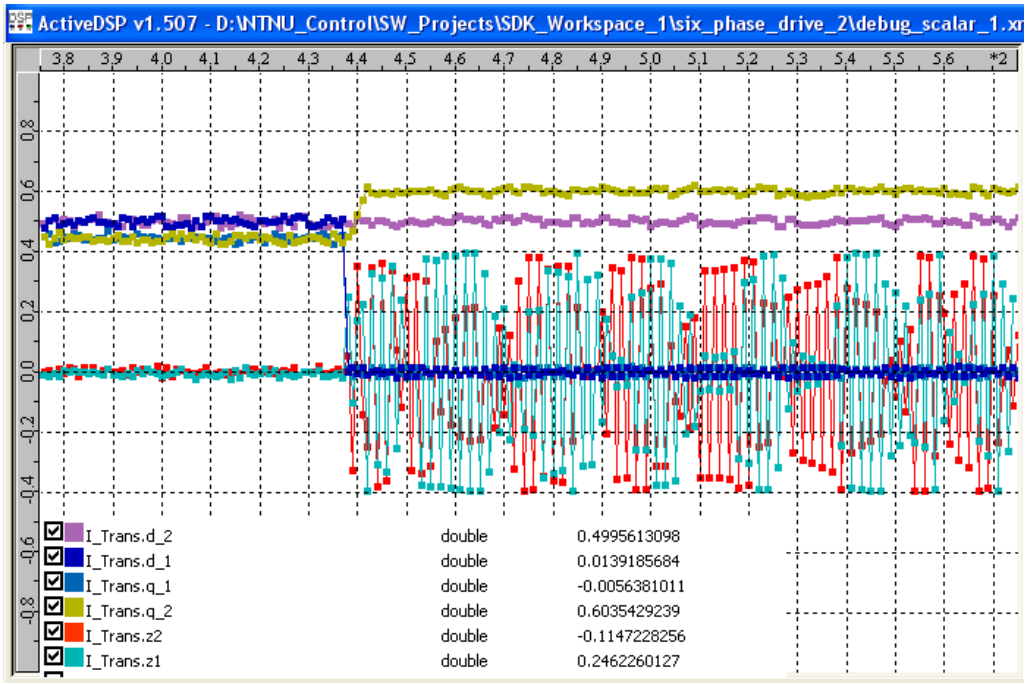


**Figure 7-8: The trip of inverter 1.**

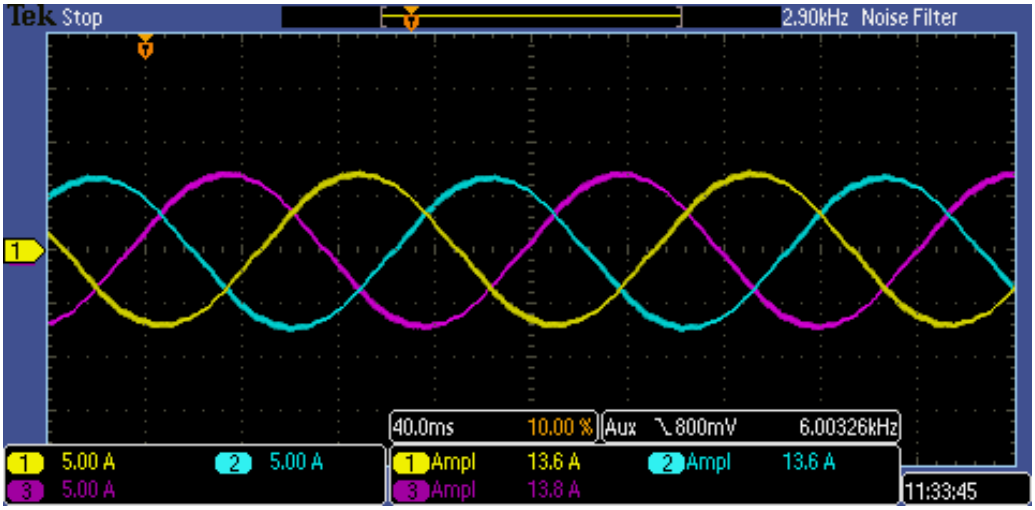


**Figure 7-9: Current in the inverter of healthy phase group.**

### *7.1.4 Operation with different DC link voltage for the Inverters.*

In the actual operation of the drive the two inverters will have change in their share of the d-q currents due to the change in the DC link voltage supplied by the converters. This condition is also tested on the actual drive.

The results for the simulation in case of the different DC link voltage are as shown in the Figure 7-10.

There is torque limiter chain included in the simulations so the simulated conditions are not exactly as carried out on the machine.

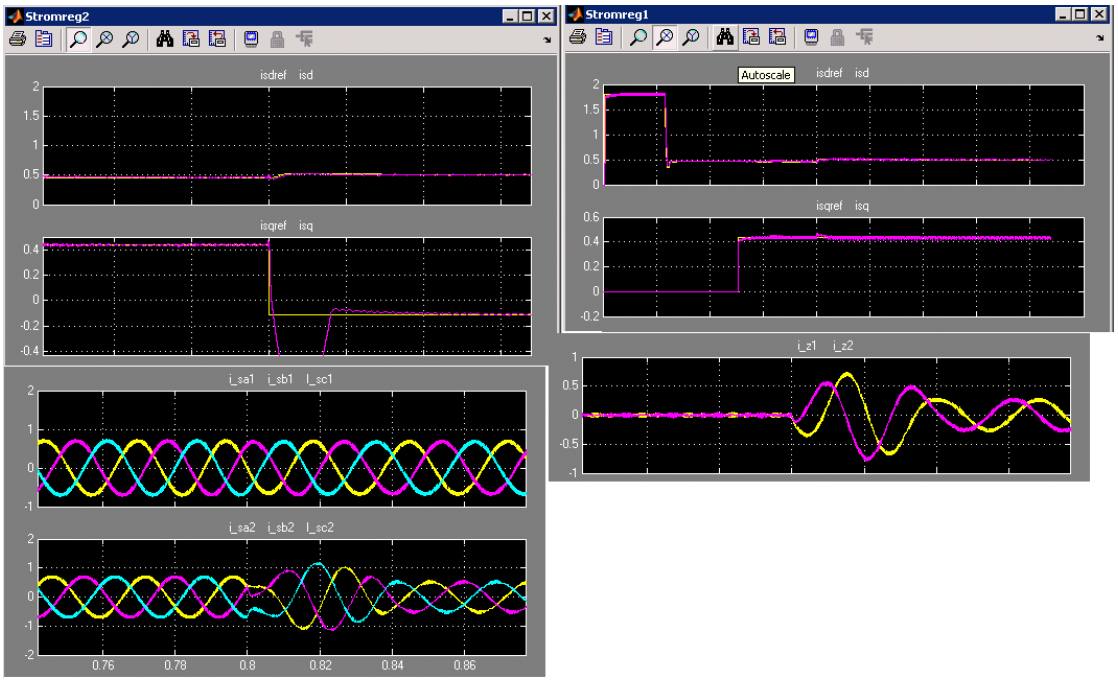


**Figure 7-10: Simulation results for operation with different DC link**

It can be seen from the simulation results the when there is step change in the DC link voltage the transient currents can be observed in the inverters if the DC link voltage changes suddenly this may cause the heavy transient currents .

While testing on the actual drive it was not possible to produce step change in the DC link voltage as the autotransformer is used to supply the DC links; however the DC link voltage of the inverter 1 was reduced to check the reduced DC link operation.

The result is as shown in the Figure 7-11. The voltage of the dc link of the inverter 1 is reduced to 90 Volts from 320 Volts. It was observed that the inverter 1 was saturated from the modulation index and from the line currents of the phase group 1 in the Figure 7-12.

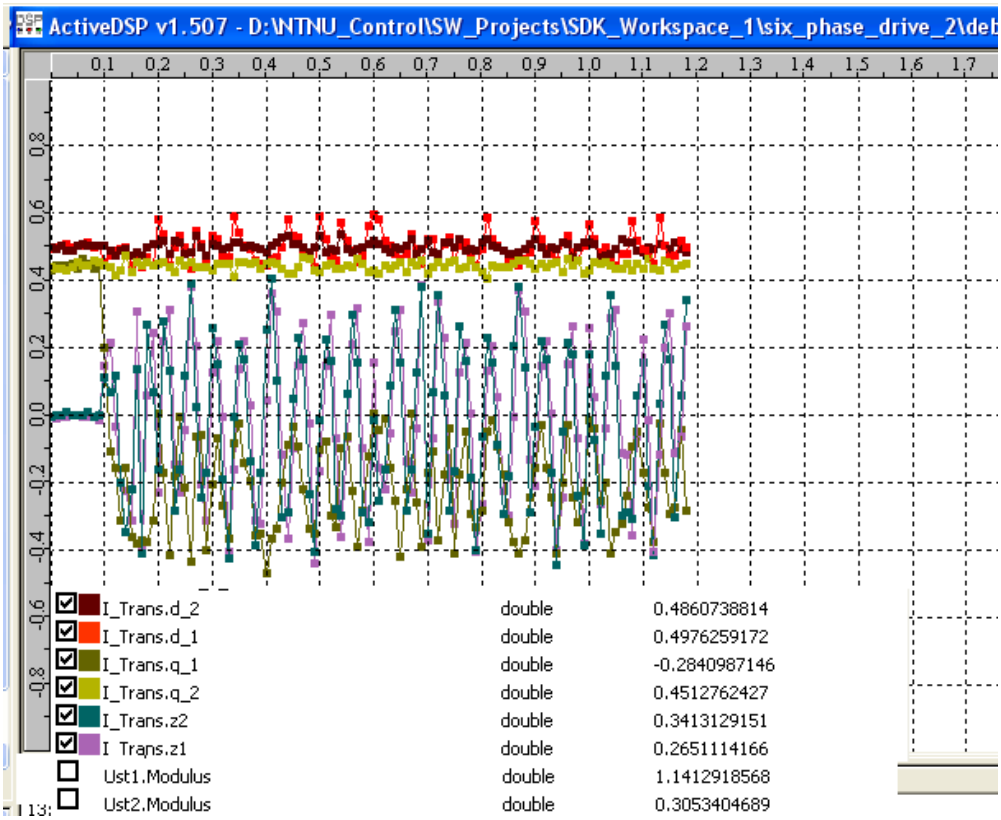


**Figure 7-11: Different DC link Voltage operation**

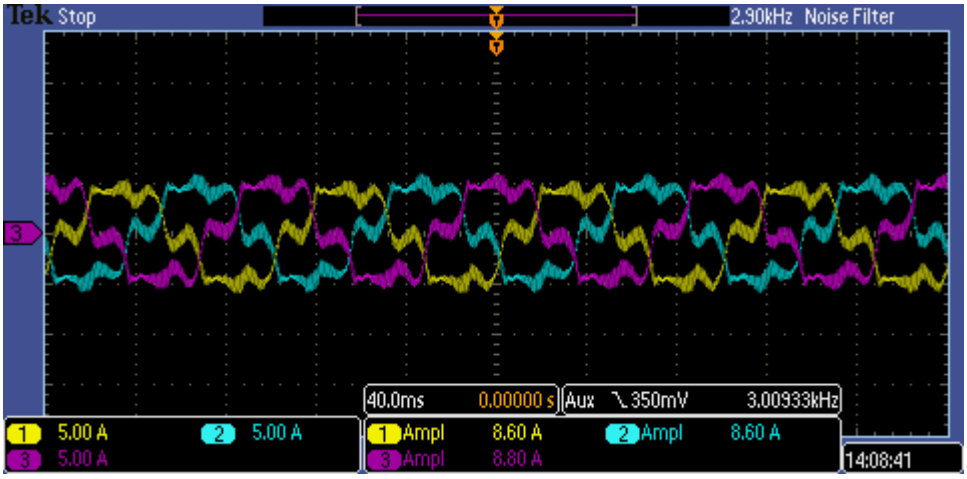


**Figure 7-12: Line currents in the inverter with reduced DC link.**

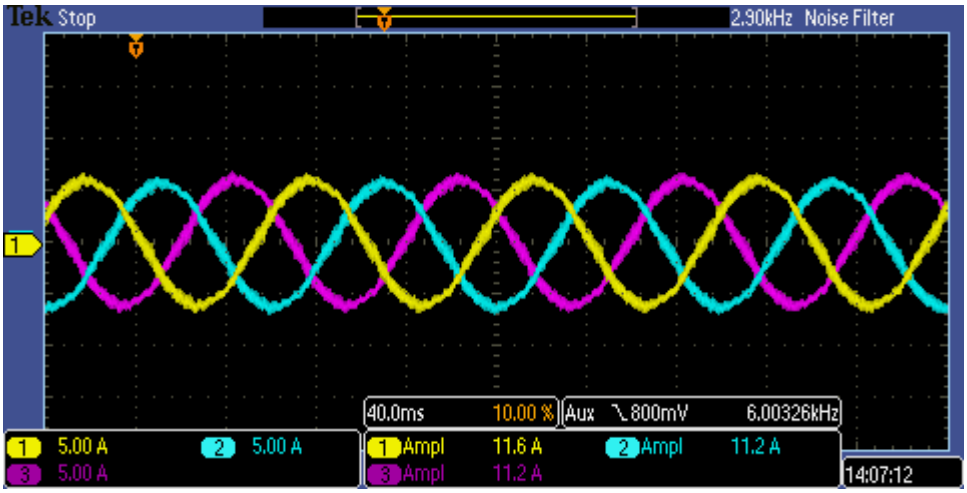


**Figure 7-13 : Line currents of the other inverter**

### *7.1.5 Start with single phase group of the SPIM.*

The DSFCC scheme can start the SPIM as with one inverter. This was observed during testing. The pulses to one of the inverters are disabled and machine was started on light load. The result of the operation can be seen in the figure however the z system currents were found as high as 0.5 pu refer Figure 7-14.

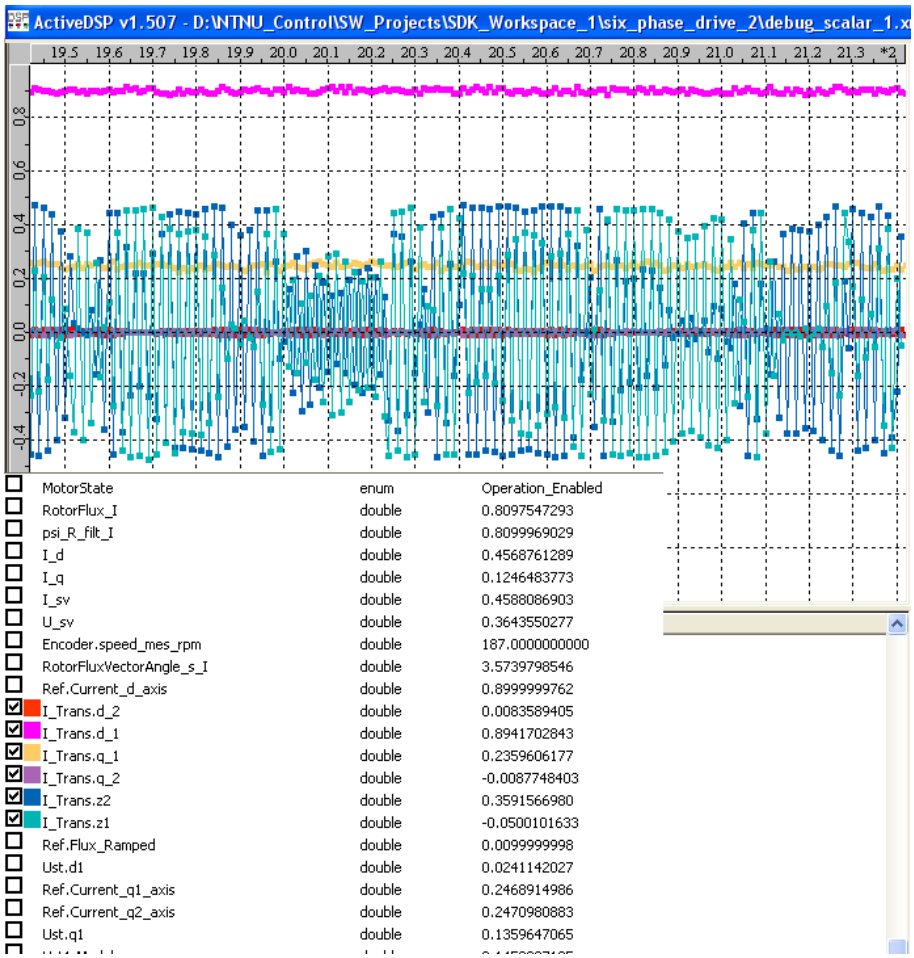


**Figure 7-14: Start with single phase group of the SPIM.**

## 7.2. The DCC strategy.

In following subsections results of the DCC strategy on the SPIM are discussed. The DCC strategy was particularly tested for the extreme cases i.e. trip of the one inverter and the low DC link voltage operation as the normal operation of the DCC strategy was found same as that of DFSCC.

### *7.2.1 Trip of one of the inverter.*

It was observed that during the trip of the one inverter the DCC strategy fails to run the SPIM as the three phase machine. The trip of the other inverter was observed even if at low loads. The current trace of the healthy inverter is as shown in the figure below.

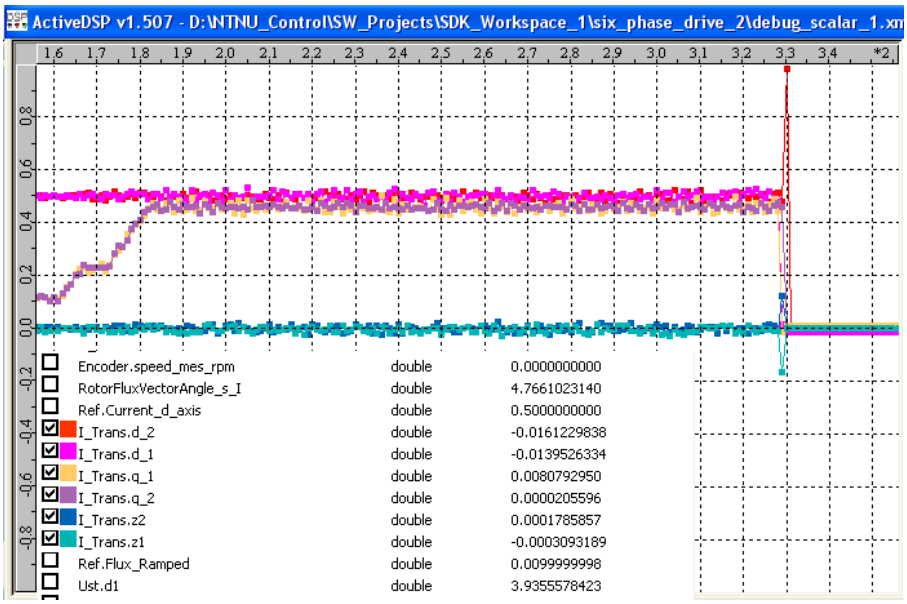


**Figure 7-15 : Trip of the inverter 1. DSP log.**

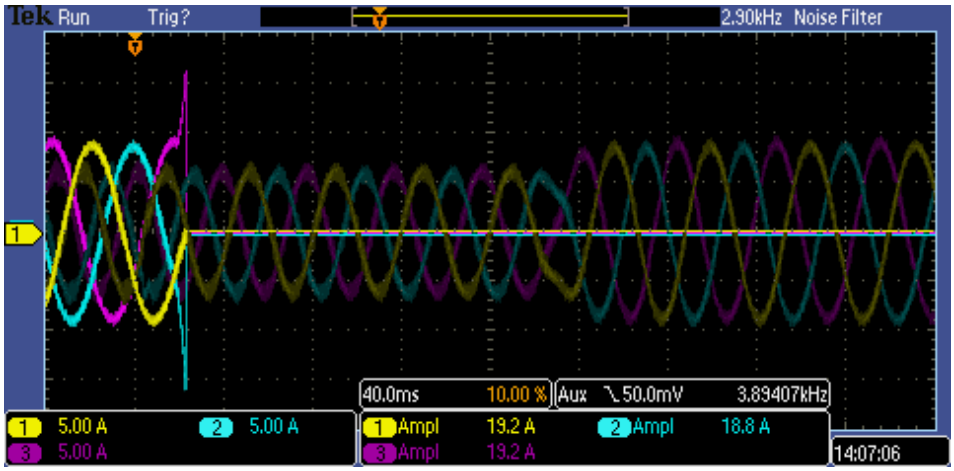

**Figure 7-16 : Trip of healthy inverter as recorded on oscilloscope.**

### *7.2.2 Low DC link voltage operation*

For the DCC in case of the low DC link voltage for one inverter it was observed that the z controllers try to control z subspaces currents as can be seen from the imbalance in the system , however when the DC link voltage becomes too low the system is tripped as can be seen from the Figure 7-17

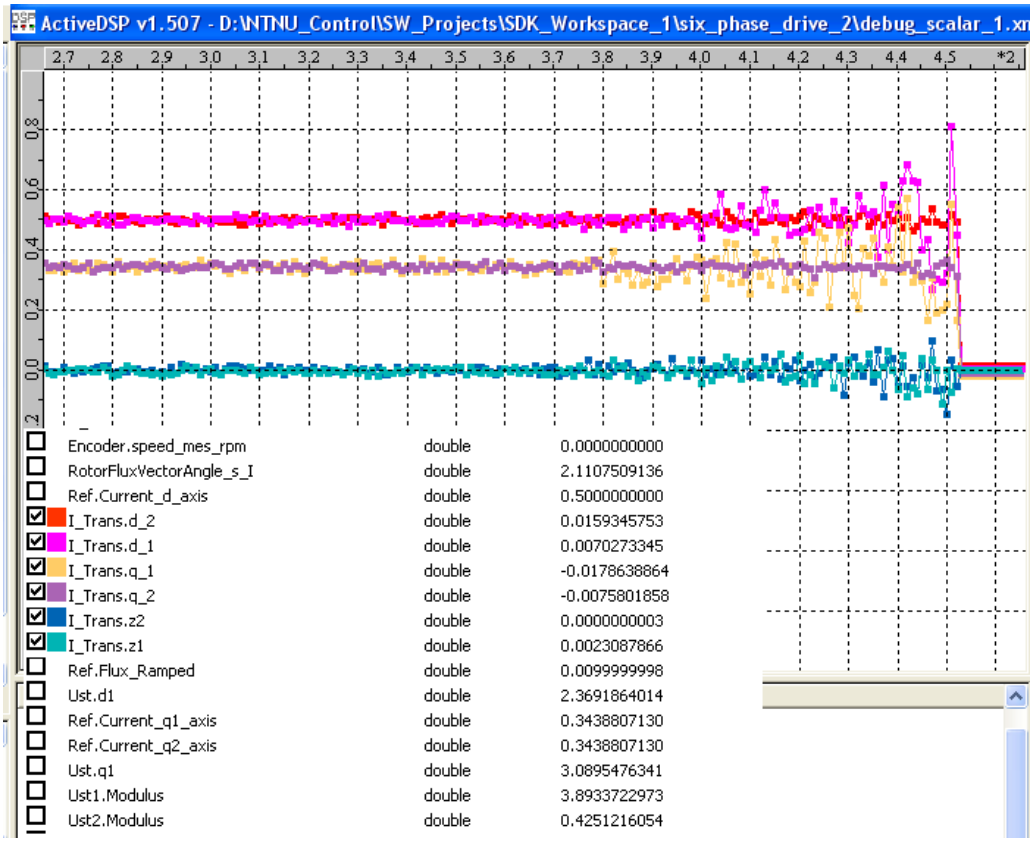


**Figure 7-17: Different DC link operation DCC strategy**

### *7.2.3 Start with the single phase group.*

The SPIM was tried to start with the only one of the inverter, it is observed that the drive cannot be started with just one inverter using this control scheme.

# 8. Summery and Conclusion.

In the thesis the two control strategies, Double Synchronous Frame Current Control and The Decoupled Current control are implemented and evaluated. The FPGA control card is programmed accordingly.

The results obtained in the simulations and the actual results that are observed on the SPIM drive for the DSFCC strategy are in agreement. The operations of the control strategies during the extreme conditions were tested such as the trip of the one inverter.

It was observed that the PI regulators are able to regulate the currents in both the control schemes, however in the DCC strategy the controllers cannot control the huge imbalance between the two inverters and the system trips same is true if the DC link voltage falls too much.

For the DSFCC strategy the SPIM drive operation is still possible even if one inverter is failed during the operation, this is possible in case if the SPIM is loaded below the rated and the inverter has sufficient overcurrent capacity.

The two control strategies are more or less gives equal performance in the steady state but in the transient state there are more z axis currents are induced in the DSFCC strategy than the DCC strategy as the DCC employs the Z axis regulator.

From the results it can be concluded that both control strategies can be complementary to each other for example in case of the failure of the one inverter on board the DSFCC control strategy can be used for the start of the machine with one inverter. While in normal operation DCC control can be used.

## 9. Further work.

In the thesis work the two control strategies were implemented and evaluated to study the actual behaviour of the two control schemes in the steady state as well as in the transient state.

The further work consists of adding the DC link torque limiting chain and the speed torque limiting chain in the drive to check the performance under the limiting conditions.

For the drive it is necessary to have online estimation of the parameters so that the vector control could be more accurate. So the program for online estimation of the SPIM parameters needs to be written and implemented.

It is interesting to see if the harmonics in the drive can be reduced with application of SVM and with increased frequency of the switching.

This work will continue during this summer.

## References.

***Publications, Thesis , Technical Documents.***

[1] **Williamson S., Smith S.** *'Pulsating Torque and losses in multiphase induction machines*.'0-7803-7116-X/01 -2001 IEEE.

[2] **Levi E. Bojoi R., Profumo F. Toliyat H.A., Williamson S. "***Multiphase induction motor drives- a technology status review."* IET Electr. Power Appl., 2007, 1(4), pp 489-516

[3] **Nelson R.H., Krause P.C.,** '*Induction machine analysis for arbitrary displacement betweenmultiple winding sets'*, IEEE Trans. Power Apparatus Syst. PAS-93 (1974) 841–848.

[4] **R. F. Schiferl, C. M. Ong**. *'Six phase synchronous machine with ac and dc stator connections-Part II: Harmonic Studies and a Proposed Uninterruptible Power Supply Scheme'*.IEEE Transactions on Power Apparatus and Systems, Vol. PAS-102, No. 8, August 1983.

[5] **M.A. Abbas, R. Christen, T.M. Jahns**, *'Six-phase voltage source inverter driven induction motor'*.IEEE Trans. Ind. Appl. IA-20(5) (1984) 1251–1259.

[6] **Singh, G.K.** 'Multi-phase induction machine drive research – a survey', Electr. Power Syst. Res., 2002, 61, pp. 139–14

[7] **Klingshirn, E.A.** *'High phase order Induction motors-Part I and II*, IEEE Trans. Power App. Syst., vol PAS-102, no.1 Jan 1983.

[8] **Zaho, Y., Lipo, T.A.** '*Space Vector PWM Control of Dual Three Phase Induction Machine Using Vector Space Decomposition'*, IEEE Trans. Ind. Applications, Vol. 31,No. 5, pp.1100-1109, Sept./Oct 1995.

[9] **Nilsen Roy** *'Distributed three phase control of six phase motors'*, Wartsila Norway, Ship Power Techonology R&D July 2008.

[10] **Bojoi R., Tenconi A., Profumo F., Griva G., Martinello D.** '*Complete Analysis and Comparative Study of Digital Modulation Techniques for Dual Three-phase AC Motor Drives'*. 0-7803-7262-X/2002 IEEE.

[11] **Bakhshai A.R., Joos *G.* and Jin H.** '*Space Vector PWM Control of a Split-Phase Induction Machine Using The Vector Classification Technique*'. *Conf Rec. Applied Power Electronics Conference and Exposition APEC* 1998, V01.2, pp.802-808

[12] **Øivind Hoem**. '*Control Of Six-Phase Machines – Master Thesis'*. NTNU June 2010.

[13] **K. Gopakumar, V. T. Ranganathan, and S. R. Bhat,** *'Split-phase induction motor operation from PWM voltage source inverter,'* IEEE Trans. Ind. Applicat., vol. 29, no. 5, pp. 927-932, Sept./Oct. 1993

[14] **R. Bojoi, E. Levi, F. Farina, A. Tenconi and F**. **Profumo**.*'Dual three-phase induction motor drive with digital current control in the stationary reference frame.'* IEE Proc.-Electr. Power Appl., Vol. 153, No. 1, January 2006.

[15] **Roy Nilsen.** *'Modelling of multi-phase synchronous machines.'*, Wartsila Norway, Ship Power Techonology R&D April 2006.

[16] **Kjell Ljøkelsøy**. *'Prosessorkort basert på Xilinx Virtex5 FPGA. V1. 1. Beskrivelse.'* SINTEF Dec. 2009.

[17] **Kjell Ljøkelsøy.** *'FPGA based processor board.'* power point presentation'.

[18] **Kjell Ljøkelsøy.***'20 kW IGBT omformer. Beskrivelse'*. SINTEF Sept 2002.

[19] **Kjell Ljøkelsøy**. *'Control system for a three-phase grid connected converter. Description.'* SINTEF Energi AS. Feb. 2011.

[20] **Tom Nestli**. *'Modelling and Identification of Induction Machines'.* Department of Electric Power Engineering. ISBN 82-7119-881-5. NTNU December 1995.

[21] **Sachin Thopate.** *'Modeling and Control of Six Phase Induction Motor'*. Department of Electric Power Engineering NTNU December 2010.

[22] **DRIVECOM.** '*Drive Engineering /Servo Blomberg, Germany.'* September 1994.

***Books.***

[B.1] **Werner Leonhard.** *'Control Of Electrical Drives'* ISBN: 3-540-41820-2. Springer 2001.

[B.2] **Bimal K. Bose.** *'Power Electronics and Variable Frequency Drives'*. ISBN: 0-7803-1084-5. IEEE Press, New York 2001.

[B.3] **Roy Nilsen. '***TET 4120 Compandium Elektriske Motordrifter'*.Department of Electric Power Engineering NTNU 2004.

[B.4] **Nguyen Qung, JorgDittrich**. 'Vector Control Of Three-Phase AC Machine-System Development in the Practice'. ISBN 978-3-540-79028-0. Springer Berlin.

***Web Link***

**[W. 1]** http://www.ece.umn.edu/users/riaz/animations/sinwaves0.html

# Appendix.

# 1. Machine parameters.

Voltage, current, resistance and flux linkage vectors for physical model

$$[\boldsymbol{U_s}] = \begin{bmatrix} \underline{U}_{sa_1} \\ \underline{U}_{sb_1} \\ \underline{U}_{sc_1} \\ \underline{U}_{sa_2} \\ \underline{U}_{sb_2} \\ \underline{U}_{sc_2} \end{bmatrix} , [\boldsymbol{I_s}] = \begin{bmatrix} \underline{I}_{sa_1} \\ \underline{I}_{sb_1} \\ \underline{I}_{sc_1} \\ \underline{I}_{sa_2} \\ \underline{I}_{sb_2} \\ \underline{I}_{sc_2} \end{bmatrix} , [\boldsymbol{I_r}] = \begin{bmatrix} \underline{I}_{ra_1} \\ \underline{I}_{rb_1} \\ \underline{I}_{rc_1} \\ \underline{I}_{ra_2} \\ \underline{I}_{rb_2} \\ \underline{I}_{rc_2} \end{bmatrix} [\boldsymbol{\Psi_s}] = \begin{bmatrix} \Psi_{sa1} \\ \Psi_{sb1} \\ \Psi_{sc1} \\ \Psi_{sa2} \\ \Psi_{sb2} \\ \Psi_{sc2} \end{bmatrix}, [\boldsymbol{\Psi_r}] = \begin{bmatrix} \Psi_{ra1} \\ \Psi_{rb1} \\ \Psi_{rc1} \\ \Psi_{ra2} \\ \Psi_{rb2} \\ \Psi_{rc2} \end{bmatrix}$$

$$[R_s] = diag[R_s] \qquad [R_r] = diag[R_r]$$

**A 1**

Self inductances of physical model

$$\boldsymbol{L_{ss}} = L_{\sigma s} \begin{bmatrix} 1 & 0 & 0 & 0 & 0 & 0 \\ 0 & 1 & 0 & 0 & 0 & 0 \\ 0 & 0 & 1 & 0 & 0 & 0 \\ 0 & 0 & 0 & 1 & 0 & 0 \\ 0 & 0 & 0 & 0 & 1 & 0 \\ 0 & 0 & 0 & 0 & 0 & 1 \end{bmatrix} + L_h \begin{bmatrix} 1 & \frac{\sqrt{3}}{2} & -\frac{1}{2} & -\frac{\sqrt{3}}{2} & -\frac{1}{2} & 0 \\ \frac{\sqrt{3}}{2} & 1 & 0 & -\frac{1}{2} & -\frac{\sqrt{3}}{2} & -\frac{1}{2} \\ -\frac{1}{2} & 0 & 1 & \frac{\sqrt{3}}{2} & -\frac{1}{2} & -\frac{\sqrt{3}}{2} \\ -\frac{\sqrt{3}}{2} & -\frac{1}{2} & \frac{\sqrt{3}}{2} & 1 & 0 & -\frac{1}{2} \\ 0 & -\frac{\sqrt{3}}{2} & -\frac{1}{2} & 0 & 1 & \frac{\sqrt{3}}{2} \\ 0 & -\frac{1}{2} & -\frac{\sqrt{3}}{2} & -\frac{1}{2} & \frac{\sqrt{3}}{2} & 1 \end{bmatrix}$$

**A 2**

$$\boldsymbol{L_{rr}} = L_{\sigma r} \begin{bmatrix} 1 & 0 & 0 & 0 & 0 & 0 \\ 0 & 1 & 0 & 0 & 0 & 0 \\ 0 & 0 & 1 & 0 & 0 & 0 \\ 0 & 0 & 0 & 1 & 0 & 0 \\ 0 & 0 & 0 & 0 & 1 & 0 \\ 0 & 0 & 0 & 0 & 0 & 1 \end{bmatrix} + L_h \begin{bmatrix} 1 & \frac{\sqrt{3}}{2} & -\frac{1}{2} & -\frac{\sqrt{3}}{2} & -\frac{1}{2} & 0 \\ \frac{\sqrt{3}}{2} & 1 & 0 & -\frac{1}{2} & -\frac{\sqrt{3}}{2} & -\frac{1}{2} \\ -\frac{1}{2} & 0 & 1 & \frac{\sqrt{3}}{2} & -\frac{1}{2} & -\frac{\sqrt{3}}{2} \\ -\frac{\sqrt{3}}{2} & -\frac{1}{2} & \frac{\sqrt{3}}{2} & 1 & 0 & -\frac{1}{2} \\ 0 & -\frac{\sqrt{3}}{2} & -\frac{1}{2} & 0 & 1 & \frac{\sqrt{3}}{2} \\ 0 & -\frac{1}{2} & -\frac{\sqrt{3}}{2} & -\frac{1}{2} & \frac{\sqrt{3}}{2} & 1 \end{bmatrix}$$

**A 3**

## Mutual Inductances

$$\boldsymbol{L_{sh}} = L_h \begin{bmatrix} cos(\theta_r) & cos\left(\theta_r + \frac{\pi}{6}\right) & cos\left(\theta_r + \frac{4\pi}{6}\right) & cos\left(\theta_r + \frac{5\pi}{6}\right) & cos\left(\theta_r + \frac{8\pi}{6}\right) & cos\left(\theta_r + \frac{9\pi}{6}\right) \\ cos\left(\theta_r + \frac{11\pi}{6}\right) & cos(\theta_r) & cos\left(\theta_r + \frac{3\pi}{6}\right) & cos\left(\theta_r + \frac{4\pi}{6}\right) & cos\left(\theta_r + \frac{7\pi}{6}\right) & cos\left(\theta_r + \frac{8\pi}{6}\right) \\ cos\left(\theta_r + \frac{8\pi}{6}\right) & cos\left(\theta_r + \frac{9\pi}{6}\right) & cos(\theta_r) & cos\left(\theta_r + \frac{\pi}{6}\right) & cos\left(\theta_r + \frac{4\pi}{6}\right) & cos\left(\theta_r + \frac{5\pi}{6}\right) \\ cos\left(\theta_r + \frac{7\pi}{6}\right) & cos\left(\theta_r + \frac{8\pi}{6}\right) & cos\left(\theta_r + \frac{11\pi}{6}\right) & cos(\theta_r) & cos\left(\theta_r + \frac{3\pi}{6}\right) & cos\left(\theta_r + \frac{4\pi}{6}\right) \\ cos\left(\theta_r + \frac{4\pi}{6}\right) & cos\left(\theta_r + \frac{5\pi}{6}\right) & cos\left(\theta_r + \frac{8\pi}{6}\right) & cos\left(\theta_r + \frac{9\pi}{6}\right) & cos(\theta_r) & cos\left(\theta_r + \frac{\pi}{6}\right) \\ cos\left(\theta_r + \frac{3\pi}{6}\right) & cos\left(\theta_r + \frac{4\pi}{6}\right) & cos\left(\theta_r + \frac{7\pi}{6}\right) & cos\left(\theta_r + \frac{8\pi}{6}\right) & cos\left(\theta_r + \frac{11\pi}{6}\right) & cos(\theta_r) \end{bmatrix}$$

$$\boldsymbol{L_{rh}} = L_h \begin{bmatrix} cos(\theta_r) & cos\left(\theta_r + \frac{\pi}{6}\right) & cos\left(\theta_r + \frac{4\pi}{6}\right) & cos\left(\theta_r + \frac{5\pi}{6}\right) & cos\left(\theta_r + \frac{8\pi}{6}\right) & cos\left(\theta_r + \frac{9\pi}{6}\right) \\ cos\left(\theta_r + \frac{11\pi}{6}\right) & cos(\theta_r) & cos\left(\theta_r + \frac{3\pi}{6}\right) & cos\left(\theta_r + \frac{4\pi}{6}\right) & cos\left(\theta_r + \frac{7\pi}{6}\right) & cos\left(\theta_r + \frac{8\pi}{6}\right) \\ cos\left(\theta_r + \frac{8\pi}{6}\right) & cos\left(\theta_r + \frac{9\pi}{6}\right) & cos(\theta_r) & cos\left(\theta_r + \frac{\pi}{6}\right) & cos\left(\theta_r + \frac{4\pi}{6}\right) & cos\left(\theta_r + \frac{5\pi}{6}\right) \\ cos\left(\theta_r + \frac{7\pi}{6}\right) & cos\left(\theta_r + \frac{8\pi}{6}\right) & cos\left(\theta_r + \frac{11\pi}{6}\right) & cos(\theta_r) & cos\left(\theta_r + \frac{3\pi}{6}\right) & cos\left(\theta_r + \frac{4\pi}{6}\right) \\ cos\left(\theta_r + \frac{4\pi}{6}\right) & cos\left(\theta_r + \frac{5\pi}{6}\right) & cos\left(\theta_r + \frac{8\pi}{6}\right) & cos\left(\theta_r + \frac{9\pi}{6}\right) & cos(\theta_r) & cos\left(\theta_r + \frac{\pi}{6}\right) \\ cos\left(\theta_r + \frac{3\pi}{6}\right) & cos\left(\theta_r + \frac{4\pi}{6}\right) & cos\left(\theta_r + \frac{7\pi}{6}\right) & cos\left(\theta_r + \frac{8\pi}{6}\right) & cos\left(\theta_r + \frac{11\pi}{6}\right) & cos(\theta_r) \end{bmatrix}$$

Voltage, current, flux linkage vectors for transformed model.

$$[\boldsymbol{U_s}^{\boldsymbol{s}}] = \begin{bmatrix} \underline{U}^s_{sd} \\ \underline{U}^s_{sq} \\ \underline{U}^s_{sz_1} \\ \underline{U}^s_{sz_2} \\ \underline{U}^s_{s0_1} \\ \underline{U}^s_{s0_2} \end{bmatrix}, [\boldsymbol{I_s}^{\boldsymbol{s}}] = \begin{bmatrix} \underline{I}^s_{sd} \\ \underline{I}^s_{sq} \\ \underline{I}^s_{sz_1} \\ \underline{I}^s_{sz_2} \\ \underline{I}^s_{s0_1} \\ \underline{I}^s_{s0_2} \end{bmatrix}, [\boldsymbol{\Psi_s}] = \begin{bmatrix} \underline{\Psi}^s_{sd} \\ \underline{\Psi}^s_{sq} \\ \underline{\Psi}^s_{sz_1} \\ \underline{\Psi}^s_{sz_2} \\ \underline{\Psi}^s_{s0_1} \\ \underline{\Psi}^s_{s0_2} \end{bmatrix}, \quad \textbf{A 4}$$

Inductance matrix for transformed model

$$\boldsymbol{L_{ss}} = \begin{bmatrix} L_{ds,ds} & L_{ds,qs} & L_{ds,dr} & L_{ds,qr} \\ L_{qs,ds} & L_{qs,qs} & L_{qs,dr} & L_{qs,qr} \\ L_{dr,ds} & L_{dr,qs} & L_{dr,dr} & L_{dr,qr} \\ L_{qr,ds} & L_{qr,qs} & L_{qr,dr} & L_{qr,qr} \end{bmatrix} + L_h \begin{bmatrix} L_s & 0 & M\,cos(\theta_r) & -M\sin(\theta_r) \\ 0 & L_s & M\sin(\theta_r) & M\,cos(\theta_r) \\ M\,cos(\theta_r) & M\sin(\theta_r) & L_r & 0 \\ -M\sin(\theta_r) & M\,cos(\theta_r) & 0 & L_r \end{bmatrix}$$

Where

$M = L_h$

$L_s = L_{s\sigma} + L_h \qquad , L_r = L_{r\sigma} + L_h$

# 2. Hardware Configurations

## 2.1 Inverter Technical Data.

• DC voltage: 0-640V.
• Capacitors: 3300 uF 350V. 2 strings of 2 capacitors in series. 47 kΩ voltage sharing resistance per capacitor

• Short circuit protection: Turning off the 400-600A
• Switching Frequency: 0-25 kHz, 0% -100% modulation.
• Power Capabilities in continuous operation: Limited by cooling: 560W losses. Tj = 110 ° C Thurs transistors in 99% modulation, the DC operation, no diode rectifier. Transient power capability is defined as the power that gives temperature (80 ° C) at Tj = 125 ° C. Given in parentheses.

45 (80) A at 300V DC, 20 kHz switching
70 (105) A at 300V DC, 10 kHz (measured 67 ADC without disconnection for over temp.)
95 (120) A at 300V DC, 5 kHz
110 (130) A at 300V DC, 2 kHz
25 (55) A at 500VDC, 20 kHz switching
50 (90) A at 500VDC, 10 kHz
80 (105) A at 500VDC, 5 kHz
105 (125) A at 500VDC, 2 kHz
• Control Signals: 5V CMOS, the signal ground potential, separated from the power circuit.
• Cooling: Air-cooled: Flange: Fischer LA V 10-300 Activation of fan: 50 ° C Cut-off : 80 ° C Cooling capacity: 560W at 45 ° C temperature rise (estimated). Forced air cooling
• Transistors:
Semikron SKM400GB125D 2x 400A 1200V IGBT Bridge leg module .
Fast transistors with relatively high lead voltage drops.
• Snubbere: 10 nF capacitive snubber and 22 nF / 1 Ohm RC snubber in parallel with the DC terminals on each Bridge leg module

**Status codes for inverter**

Status codes indicate the cause of the converter is blocked. In case of multiple errors, errors with the highest number are shown. Possible use of available inputs is indicated in parentheses.

Status Code:

F +5 V low / delayed start
E protection transistor A + Trip
D protection transistor B + Trip
C protection transistor C+ Trip
B Protection braking transistor Trip
A protective transistor A- Trip
9 protection transistor B- trip
8 Protection transistor C-trip
7 (Signal 7) (Power Over current).
6 Over temperature of cooling fins
5 (Signal 5) (Over Temperature rectifier)
4 (Signal 4)
3 Overvoltage DC-link
2 (Signal 2) (External interlocking / blocking)
1 (signal 1, (main contacts open, charging the DC link.)
0 OK, Ready. No blocking. (Green LED lights up.)

Status codes are also available for the control unit via the connection socket driver (PWM connector). Inverted logic, active low, is used here to avoid the error signals to the control device when using power electronics converter is off.

## 3. Per Unit system and Motor Parameters

In the control of Induction machine all the values are used in the per unit . The per unit scaling factors used are as shown below.

| Parameter | Scaling Factor | Per unit quantity |
|---|---|---|
| Voltage | $\sqrt{2}\hat{U}_n$ | $u = \frac{U}{\sqrt{2}\hat{U}_n}$ |
| Current | $\sqrt{2}\hat{I}_n$ | $i = \frac{I}{\sqrt{2}\hat{\imath}_n}$ |
| Resistence, Reactance | $Z_n = \frac{\hat{U}_n}{\hat{I}_n}$ | $r = \frac{R}{Z_n}$ , $x = \frac{X}{Z_n}$ |
| Angulr Speed | $\omega_n = 2\pi f_n$ | $f = \frac{\omega}{\omega_n}$ |
| Frequency | $f_n$ | $f = \frac{f_{Hz}}{f_n}$ |
| Speed | $n_n = 60\frac{f_n}{p}$ | $n = \frac{N_{rpm}}{n_n}$ |
| Power | $S_n = 3.(\hat{U}_n.\hat{I}_n)$ | $S = \frac{S_{VA}}{S_n}$ |
| Torque | $m_e = \frac{S_n.p}{\omega_n}$ | $m = \frac{M}{M_n}$ |
| Flux Linkage | $\psi_n = \frac{\sqrt{2}\hat{U}_n}{\omega_n}$ | $\psi = \frac{\Psi}{\psi_n}$ |

For the vector control of the Induction Motor the motor parameters are calculated from the name plate data as below.

It can be shown that [B.4]

$$\hat{\imath}_{sd} = \sqrt{1 - \cos\varphi}$$ **A 5**

$$\hat{\imath}_{sq} = \sqrt{\cos\varphi}$$ **A 6**

From the approximate phasor diagram of the Induction machine

$$\sin\gamma = \sin(\varphi - (90 - \alpha))$$

$$\sin\gamma = \sin\varphi.\sin\alpha - \cos\varphi.\cos\alpha$$

$$\sin\gamma = \sin\varphi.\hat{\imath}_{sd} - \cos\varphi.\hat{\imath}_{sq}$$ **A 7**

Value of

$$\cos\varphi = 0.77$$

From A 7

$$\sin\gamma = 0.1927$$

The leakage reactance value can be approximated by

$$x_\sigma \cong \frac{\sin\gamma}{\hat{\imath}_{sq}}$$

$$x_\sigma = 0.2196 \text{ pu.}$$ **A 8**

This is fairly accurate.

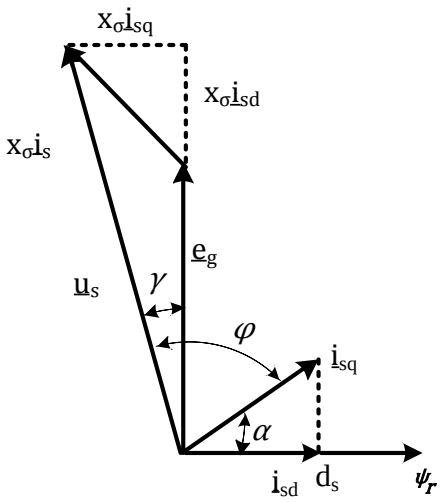


**Figure-A 1: Approximate phasor diagram [B.4]**

The main reactance can be written as

$$x_h \cong \frac{1}{\hat{\imath}_{sd}} - x_\sigma$$

$$x_h \cong 1.865 \text{ pu}$$

The leakage coefficient

$$\sigma \cong \frac{x_\sigma}{x_h}$$

The rotor resistance is assumed to be equal to the rated slip

$$r_r \cong 0.0066$$

$$T_r \cong \frac{x_r}{\omega_n . r_r}$$

$$T_r \cong 0.6380 \text{ sec}$$

## 4. PI Regulator Parameters.

When the PI regulators are introduced in the stator voltage equations (3-20) the transfer functions for the various currents can be written after introducing the serial gain equal to the inverse of the DC link voltage as

$$h_{oid} = \frac{i_d}{i_d^*} = k_{pd}.\left(\frac{1+T_{id}.s}{T_{id}.s}\right)\left(\frac{\omega_n T_d}{(1+T_d.s).(1+T_{fd}.s)}\right)$$

$$h_{oid} = \frac{i_d}{i_q^*} = k_{pd}.\left(\frac{1+T_{iq}.s}{T_{iq}.s}\right)\left(\frac{\omega_n T_q}{(1+T_q.s).(1+T_{fq}.s)}\right)$$

$$h_{oid} = \frac{i_{z1}}{i_d^*} = k_{pd}.\left(\frac{1+T_{iz1}.s}{T_{iz1}.s}\right)\left(\frac{\omega_n T_{z1}}{(1+T_{z1}.s).(1+T_{fz1}.s)}\right)$$

$$h_{oid} = \frac{i_{z2}}{i_d^*} = k_{pd}.\left(\frac{1+T_{iz2}.s}{T_{iz2}.s}\right)\left(\frac{\omega_n T_{z2}}{(1+T_{z2}.s).(1+T_{fz2}.s)}\right)$$

The current controller parameters are calculated using the modulus optimum technique. As below

| Parameter | Explanation | Value |
|---|---|---|
| $K_{pd}$ | Gain in d axis current controller | 1.12 |
| $T_{id}$ | Time constant for d axis current controller | 0.04 |
| $K_{pq}$ | Gain in q axis current controller | 1.12 |
| $T_{iq}$ | Time constant for q axis current controller | 0.04 |
| $K_{pz1}$ | Gain in d axis current controller | 1.12 |
| $T_{iz1}$ | Time constant for q axis current controller | 0.04 |
| $K_{pz2}$ | Gain in q axis current controller | 1.12 |
| $T_{iz2}$ | Time constant for q axis current controller | 0.04 |

**Table 5. Controller data calculated for the simulation**

However while actual test run on the machine it is found that the inverters are tripping due to over currents so the gain of the PI regulators are reduced to 0.12

# 5. Nameplate Data of Components

## 1. Auto Transformer

Primary - 3 x 380 /220 Volts.
Secondary / 3X 0-415 / 240 Volts .
Apparent Power - 10.8 KVA
Phase group – Y0

## 2. Isolation Transformer

Primary – 230 Volts -63 Amps
Seconadary – 400 Volts- 36.1 Amps
Apparent Power - 25 kVA.

# 6. Software Code

The source files are too big to attach here so these files are attached outside in the DAIM .
The code developed by the author in co-operation with the SINTEF and Wartsila is available at the NTNU. This code can be used to control of normal three phase machines as well as the six phase machines. The code is being used by the Author for the Six Phase Induction Machine Control and the Nahome Ayehuni (another master student at the NTNU ) for the Six Phase PMSM control.